© 2021. Published by The Company of Biologists Ltd | Journal of Cell Science (2021) 134, jcs258603. doi:10.1242/jcs.258603

RESEARCH ARTICLE

Hherisomes, Hedgehog specialized recycling endosomes, are required for high level Hedgehog signaling and tissue growth

Sandrine Pizette[1,*], Tamás Matusek[1,*], Bram Herpers[2], Pascal P. Thérond[1,‡] and Catherine Rabouille[2,3,4,‡]

ABSTRACT

In metazoans, tissue growth and patterning is partly controlled by the Hedgehog (Hh) morphogen. Using immuno-electron microscopy on *Drosophila* wing imaginal discs, we identified a cellular structure, the Hherisomes, which contain the majority of intracellular Hh. Hherisomes are recycling tubular endosomes, and their formation is specifically boosted by overexpression of Hh. Expression of Rab11, a small GTPase involved in recycling endosomes, boosts the size of Hherisomes and their Hh concentration. Conversely, increased expression of the transporter Dispatched, a regulator of Hh secretion, leads to their clearance. We show that increasing Hh density in Hherisomes through Rab11 overexpression enhances both the level of Hh signaling and disc pouch growth, whereas Dispatched overexpression decreases high-level Hh signaling and growth. We propose that, upon secretion, a pool of Hh triggers low-level signaling, whereas a second pool of Hh is endocytosed and recycled through Hherisomes to stimulate high-level signaling and disc pouch growth. Altogether, our data indicate that Hherisomes are required to sustain physiological Hh activity necessary for patterning and tissue growth in the wing disc.

KEY WORDS: Hedgehog, *Drosophila*, Wing imaginal disc, Electron microscopy, Endocytosis, Hherisomes, Signaling, Growth, Rab11, Dispatched

INTRODUCTION

The conserved family of Hedgehog (Hh) proteins act as short- and long-range secreted morphogens, controlling tissue patterning and differentiation during embryonic development. Following synthesis in the endoplasmic reticulum, full length Hh molecules undergo an autoproteolytic cleavage to generate an Hh-N peptide and a C-terminal region (Hh-C). The Hh-N peptide has a cholesterol moiety covalently attached to its C-terminus, and a palmitic acid (saturated fatty acid) on its N-terminus. The fully lipidated Hh-N is a mature form of Hh that contains all Hh signaling activity (Pepinsky et al., 1998; Porter et al., 1995). Both modifications are necessary for correct Hh activity, as well as for Hh propagation (Briscoe and Thérond, 2013).

Hh is involved in patterning of numerous tissues, including the wing imaginal disc of *Drosophila*, the model we used in this study. The larval wing disc is an epithelium 'sac' comprising a monolayer of columnar cells (with their apical pole facing a lumen) covered by a layer of squamous cells (Fig. S1A). The columnar cells are subdivided into two populations, the posterior cells, which produce Hh (green in Fig. S1A), and anterior cells, which receive the Hh signal. Anterior and posterior cells form the anterior and posterior compartments of the wing disc, respectively. Hh patterns the anteroposterior (A/P) axis of the developing epithelial wing imaginal disc by controlling, in a non-autonomous manner, the fate of the cells present at the central part of the wing pouch in the anterior compartment. This is achieved through short- and long-range Hh signaling activity that directly activates different target gene expression.

Hh is also indirectly involved in growth stimulation by regulating the expression of the mitogenic Decapentaplegic (Dpp, the *Drosophila* homolog of BMP) morphogen at the A/P border (Basler and Struhl, 1994). Accordingly, depletion of Hh activity during larval development leads to smaller wing discs, consequently resulting in smaller adult wings after metamorphosis (Basler and Struhl, 1994).

Largely based on data gathered from the *Drosophila* wing disc, different models for Hh release and spreading in the extracellular space have been put forward. The first one shows that the active Hh peptide is secreted by the epithelial posterior cells to the plasma membrane, is then quickly re-internalised from the apical side of the same cells, and is likely recycled to the plasma membrane before release (Callejo et al., 2011; D'Angelo et al., 2015). A second set of data shows that upon decrease of endosomal sorting complex required for transport (ESCRT) activity, Hh is retained at the plasma membrane of posterior cells and loses its long-range activity (Matusek et al., 2014). This, with the finding of extracellular vesicles containing both ESCRT and Hh, suggests a role for extracellular vesicles in Hh release (Gradilla et al., 2014; Matusek et al., 2014). A third model includes cytonemes, long basal tubules that connect posterior Hh-producing cells to Hh-receiving ones. These dynamic extensions bring membrane-associated Hh to anterior receiving cells and activate them in a juxtacrine manner (Bischoff et al., 2013; Chen et al., 2017; González-Méndez et al., 2017; Sanders et al., 2013). Last, the fourth mode proposes that Hh is packaged in, and released with, lipoprotein particles (Panáková et al., 2005). The diversity of these models suggests that aspects of the release and spreading of mature Hh remain to be established, including the exact nature of the intracellular compartments involved, as well as the precise trafficking routes.

To shed light on these questions, we carried out an extensive ultrastructural approach by immuno-electron microscopy to localise Hh in the intracellular compartments of the cells of the posterior and anterior domain of the *Drosophila* larval wing imaginal disc (Fig. S1B,C). Here, we identified a membrane-bound compartment that contains 90% of intracellular Hh and that we named Hherisomes.

[1]Université Côte d'Azur, Centre National de la Recherche Scientifique (CNRS), Inserm, Institute of Biology-Valrose (iBV), 06108 Nice Cedex 2, France. [2]Section Cell Biology, Center for Molecular Medicine, University Medical Center Utrecht, 3584 CX Utrecht, The Netherlands. [3]Hubrecht Institute/KNAW [Koninklijke Nederlandsee Akademie van Wetenschap (Dutch Royal Academy of Sciences)] and UMC Utrecht, 3584 CT Utrecht, The Netherlands. [4]Biological Sciences of Cells and Systems (BSBC) Department, UMC Groningen, 9713 AV Groningen, The Netherlands.
*These authors contributed equally to this work

‡Authors for correspondence (therond@unice.fr; c.rabouille@hubrecht.eu)

S.P., 0000-0003-3193-1134; P.P.T., 0000-0003-0434-2334; C.R., 0000-0002-3663-9717

Handling Editor: Jennifer Lippincott-Schwartz
Received 2 March 2021; Accepted 7 April 2021

Journal of Cell Science (2021) 134, jcs258603. doi:10.1242/jcs.258603

Hherisomes appear to be recycling tubules emanating from endosomes. Furthermore, we showed that increasing the expression of Hh, as well as Rab11, a small GTPase involved in recycling endosomes (Ren et al., 1998; Ullrich et al., 1996), boosted Hherisome size and Hh density. Conversely, providing excess of the transporter Dispatched (Disp), a known regulator of Hh secretion (Burke et al., 1999), significantly wiped out their formation. We reveal that Hherisome formation is coupled to high Hh-signaling activity and tissue growth. Indeed, Hherisome formation through Rab11 overexpression stimulates both high level Hh signaling and disc pouch growth, whereas Disp overexpression decreases both.

RESULTS

Hherisomes are a novel Hh$^+$ membrane-bound intracellular compartment

Using immunoelectron microscopy (IEM) of *Drosophila* wild-type imaginal disc with a specific antibody against Hh followed by gold conjugation on ultrathin frozen sections, we visualised endogenous Hh, even though its detection level is very low. Hh could not readily be observed at the plasma membrane, in endosomes and in the endoplasmic reticulum (ER), but it was observed in the Golgi, in agreement with its biosynthesis route. In addition, most Hh could be detected in new intracellular membrane-bound structures. These structures were small (Table S1, 125±78 nm in diameter) dense ovoid shaped compartments that we named Hherisomes (Fig. 1A, arrows, and Fig. 1A′) (Table 1, line 1). In the posterior compartment, Hherisomes were localised both basally and apically with a 1:1 ratio (data not shown).

To allow a more detailed quantitative analysis of Hherisomes, untagged full-length Hh (HhM1 or HhM4, which are processed to its mature form as the endogenous) was overexpressed in the posterior disc compartment (where endogenous Hh is normally produced) using the binary UAS-Gal4 system (Brand and Perrimon, 1993; see Materials and Methods). Wing discs were processed for IEM, as above (Fig. 1B). The plasma membrane and multivesicular bodies (MVBs, see definition in the IEM section of Materials and Methods) were now labeled (Table 1), as well as the Golgi (Fig. 1B-B″). Importantly, the frequency of Hherisomes per cell appeared to be at least 4-fold higher than in wild-type discs (Table S1). They were enriched for Hh, (Fig. 1B-B″, arrows) displaying a 4.5 to 7-fold increased Hh labeling density (that is equivalent to concentration; see Materials and Methods for definition) when compared to endogenous Hh (Table S1; Table 1, compare line 2 for HhM4 and line 5 for HhM1 to line 1). In these discs, Hherisomes were also 1.64-fold larger than in a wild-type context (Table S1), up to 600 nm, and they occasionally contained internal membrane (Fig. 1C). Hherisomes were at the apical and the basal side of the cells with similar features, although they now appear 1.5-2.2-fold more abundant at the apical side (not shown). Overall, we estimated that 90% of intracellular overexpressed Hh was present in Hherisomes (Table 1, column Relative distribution). Note that, although most endogenous Hh was detected in Hherisomes, its low detection level did not allow us to calculate precisely its relative distribution.

Importantly, Hherisomes were not labeled for overexpressed Wg-HA, which, as for Hh, is also lipidated but with a palmitoleate (Fig. S2A, arrows). We also overexpressed secreted GFP (secGFP, Fig. S2B), as well as HhN-GFP, a GFP tag at the C-terminus of HhN that lacks the cholesterol moiety but retains the palmitate (Fig. S2C). Both SecGFP and HhN-GFP were present in Hherisomes (based on morphology), but unlike full-length Hh, they did not trigger an increase in Hherisome number and size, and the density of both in these structures was low.

To test the role of Hh lipid moieties in its enrichment in Hherisomes, we overexpressed the dually lipidated HhGFP (as in D'Angelo et al., 2015). This molecule was recruited to Hherisomes, the numbers of which increased slightly (Table S1), but was not enriched in Hherisomes, with a density therein that was close to endogenous Hh (Table S1; Fig. S2D,D′). This shows that the presence of Hh lipid moieties was not sufficient to account for its enriched incorporation in Hherisomes, and that another property of the full length that is lost in the tagged version is necessary.

Taken together, we show that Hherisomes contain the vast majority of intracellular Hh (90% of intracellular Hh). They may also contain other cargo, albeit at a much lower concentration. Furthermore, their biogenesis is specifically driven by overexpression of full-length untagged Hh.

Of note, as Hherisomes in wild-type wing discs were too few to score in a quantitative manner, all the experiments described below are performed with wing discs overexpressing full-length untagged Hh in the posterior compartment under the control of its own promotor as above, unless mentioned otherwise.

Hh$^+$ Hherisomes are not transport intermediates of the biosynthetic pathway

To determine the nature of Hherisomes and clarify whether they are part of the Hh biosynthetic pathway, we first assessed whether Hherisomes are found only in the posterior Hh-producing disc cells. If Hherisomes are an intermediate in the secretion of newly synthesised Hh, they should be specific for these cells. To unambiguously identify the posterior cells, we overexpressed an unsecreted form of GFP, cytoplasmic GFP (cytoGFP) under the control of hhGal4.

We found that Hherisomes containing Hh [either endogenous (data not shown), or overexpressed Hh] were present in both the posterior producing cells, as expected (Fig. 2A), but also in the anterior Hh-receiving cells (Fig. 2A′; Table 1, line 2 for M4, and line 5 for M1). Indeed, Hh$^+$ Hherisomes were regularly observed in the anterior compartment of the wing disc, up to 20-30 cells away from the A/P compartment border. The Hh density of the anterior compartment Hherisomes was about 2-fold lower than those of the posterior compartment (Table 1, line 2 and 5). Anterior Hherisomes appeared to be sometimes larger, but their morphological appearance was overall similar in both compartments. These results rule out that Hherisomes are biosynthetic and involved in the primary secretion of newly synthesised Hh. Instead, they suggest that Hherisomes are endocytic, likely resulting from the uptake of secreted Hh both by the posterior and the anterior cells.

To confirm this, we overexpressed Hh together with cytoplasmic GFP in the dorsal compartment of the wing disc using *apterous*Gal4 (apGal4), and then scored Hh$^+$ Hherisomes both in the dorsal and the ventral posterior disc compartments. As we did not overexpress Hh in the ventral compartment here, it should have only contained a few Hherisomes with endogenous Hh, should Hherisomes be biosynthetic. However, a boost in Hherisomes biogenesis, as well as an increase in their Hh content, was equally observed in both the dorsal (Fig. 2B) and ventral compartments (Fig. 2B′). Importantly, these Hherisomes shared the same features and characteristics in both compartments. This further indicates that Hherisome formation is downstream of Hh endocytosis.

To directly test whether the presence of Hh in Hherisomes depends on Hh endocytosis, we blocked Hh endocytosis using different means. We first expressed a dominant-negative version of Dynamin (called Shibire in *Drosophila*) but this resulted in animal lethality. Instead, we overexpressed Hh in the presence of Ptc^{1130X}, a mutated version of its receptor Patched (Ptc; Johnson et al., 2000) that cannot be internalised

Journal of Cell Science (2021) 134, jcs258603. doi:10.1242/jcs.258603

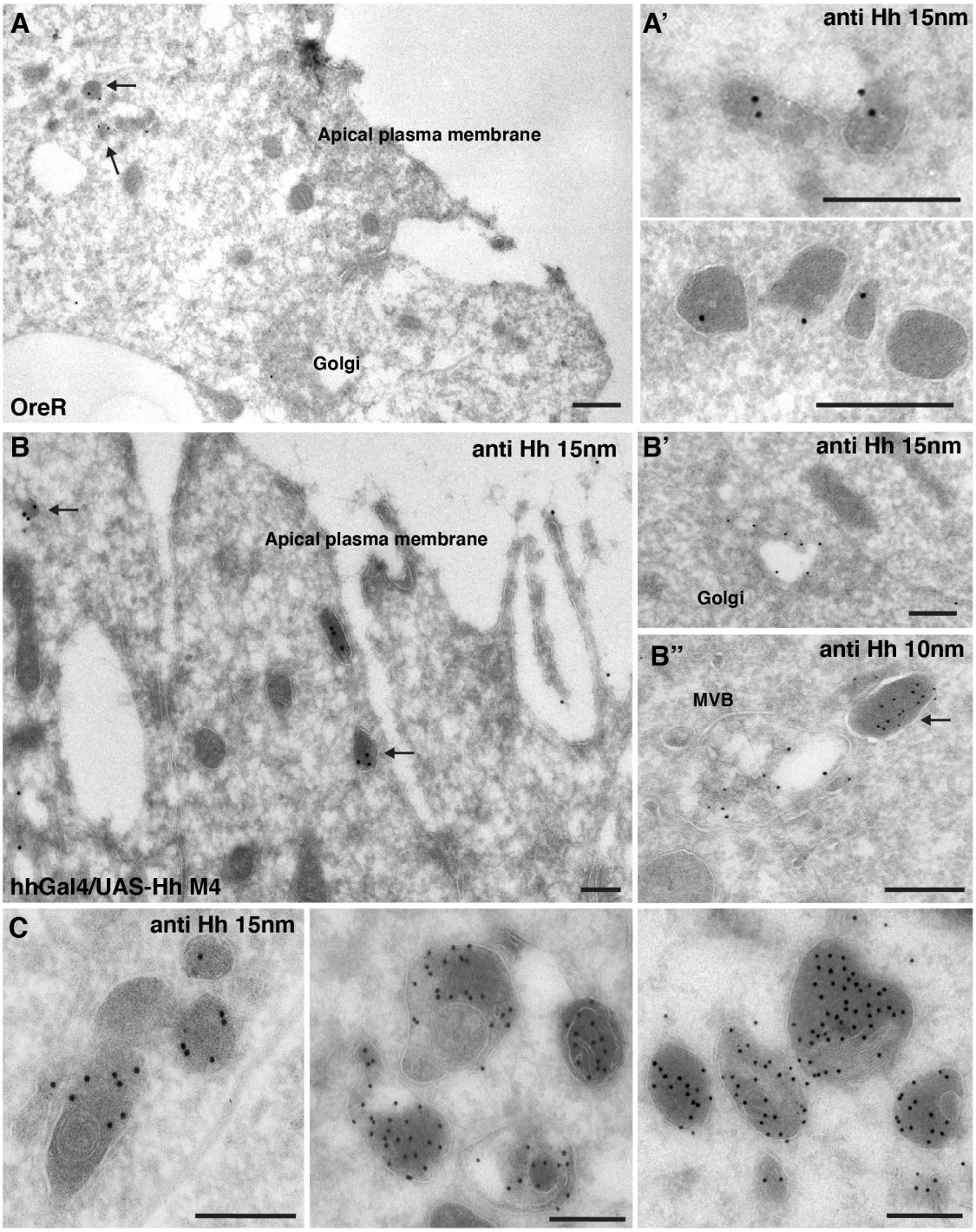

Fig. 1. Intracellular Hh is mainly localised in Hherisomes. In all IEM figures, Hh was labelled using anti-Hh antibody followed by 15 nm PAG. (A,A′) Immunolocalization of endogenous Hh wild-type (OreR) wing disc posterior cells. The Golgi and small ovoid membrane compartments (Hherisomes) (A, arrows, A′) are weakly labeled. (B-B″) Immunolocalization of overexpressed untagged Hh in posterior cells. The Golgi (B′) and Hherisomes (arrows in B and B″) are more strongly labeled than in OreR. MVBs (B″) and apical plasma membranes are also weakly positive. (C) Gallery of Hherisomes formed upon Hh overexpression. Scale bars: 200 nm.

and therefore traps Hh at the cell surface (Ayers et al., 2010). Accordingly, blocking Hh-specific endocytosis by co-expressing Ptc^{1130X} with Hh resulted in Hherisomes displaying a Hh density 2-fold lower than those in control discs (Hh overexpression alone), both at the posterior and the anterior compartment (Table 1, compare line 3 to line 2). Altogether, these results suggest that, after endocytosis, Hh traffics to Hherisomes. They also suggest that Hherisome formation depends on, and is downstream of, Hh endocytosis in both posterior and anterior compartments.

Hherisomes are not lysosomes

To place Hherisomes in the endosomal pathway, we assessed whether they are positive for markers of the endolysosome compartments. We first analysed the distribution of a dominant-negative variant of Rab5-

Journal of Cell Science (2021) 134, jcs258603. doi:10.1242/jcs.258603

Table 1. Labeling density and relative distribution of Hh in Hherisomes and MVBs

		Labeling density of Hh* (in gold/μm^2)		Relative distribution* of Hh (%)		
	Genetic background	Hherisomes	MVBs‡	Hherisomes	MVBs	Others
1	OreR	**POST:** 73.5±50 [17]§		¶		
2	hhGal4/UAS-**Hh M4<**UAS-cytoGFP	**POST:** 520±30 [59] **ANT:** 350±70 [43]				
3	UAS-Ptc^{1130X}; hhGal4/UAS-**Hh M4**	**POST:** 201±20 [58] **ANT:** 160±25 [23]				
4	UAS-DispHA; hhGal4/UAS-**Hh M4**	**POST:** very few [5] **ANT:** 142.5±40 [14]	**POST:** 4±2 [5]			
5	UAS-**Hh M1**; hhGal4/UAS-hLamp1	**POST:** 328±25 [83] **ANT:** 159±40 [32]	**POST:** 35±10 [13]	89	8	3
6	UAS-**Hh M1**; hhGal4/UAS-Rab11YFP	**POST:** 721±90 [59] **ANT:** 362±100 [66]	**POST:** 46±15 [13]	94	3	3
7	UAS-**Hh M1**; hhGal4<disp-/disp-	**POST:** 222±100 [84] **ANT:** 164±80 [71]	**POST:** 33±12 [12]	90	7	3

Bold text in the first column highlights the Hh transgene used in the experiments.

*Labeling density corresponds to the concentration of Hh per μm^2 of organelle profile in sections. The relative distribution estimates how Hh distributes over the different organelle profiles (see Materials and Methods).

‡MVBs define the endosomal profiles observed in disc cells (see Materials and Methods section).

§Numbers in brackets indicate the number of objects that were analysed over many pictures taken from different experiments.

¶Owing to the low detection of endogenous Hh in OreR, the relative distribution has not been precisely estimated.

YFP and wild-type Rab7-GFP by IEM, but this did not lead to specific signals. To analyse this further, we expressed the human lysosomal-associated membrane protein 1 (hLamp1) in the posterior compartment of the wing disc (Fig. 3A,A′). Lamp1 is a transmembrane protein that is normally concentrated in MVBs and lysosomes in mammalian cells (Galmes et al., 2015; Williams and Fukuda, 1990).

Contrary to mammalian cells in which different categories of endosomes (early and late) are clearly visible (Sachse et al., 2002), the only endosomal profiles observed in wing disc cells are vacuoles containing internal vesicles that morphologically correspond to MVBs. Based on their morphology, we have used this term to name these vacuoles. Importantly, these MVBs were all positive at a high density for overexpressed hLamp1 (Fig. 3A′). Conversely, most Hherisomes were negative for this marker (Fig. 3A), and the few that were positive displayed a hLamp1-labeling density 3-4-fold lower than MVBs. Furthermore, Hherisomes were morphologically distinct from MVBs.

Because of their electron-dense features, Hherisomes could be lysosomes. However, this is unlikely as they displayed a low concentration of Lamp1. To test this further, we monitored whether Hherisomes could be reached by endocytosed bovine serum albumin (BSA)-gold, a suitable tracer of fluid phase endocytosis reaching late endosomes and lysosomes after internalisation and chase (Sachse et al., 2002; Galmes et al., 2015). If Hherisomes correspond to these compartments, they would be reached by internalised BSA-gold under conditions in which the 100% MVBs are also labelled. As expected, 1-2 h internalisation (followed or not by 2-4 h chase) led to heavy BSA-gold accumulation in 100% of the MVBs (Fig. 3B) located at the basal side (Table S1). However, only 14-18% of the Hherisomes were weakly positive for BSA-gold (even after a long chase of the BSA-gold after internalisation) (arrows in Fig. 3B; Table S2). This was also true for wild-type background, in which Hh was not overexpressed (Fig. 3C). Critically, a similar pool of Hherisomes in anterior cells were also weakly accessible to BSA-gold (Fig. 3B′, arrows) next to strongly labeled basal MVBs. This strengthens the notion that Hherisomes, in both posterior and anterior cells, are very similar and are formed through the same pathway. Taken together, the fact that Hherisomes are weakly positive for Lamp1 and can be labeled by internalised BSA-gold confirms that they are part of the endocytic pathway. However, their low labeling density for these two markers makes it unlikely that they are either endosomes or lysosomes.

Hherisomes are not degradative compartments

As the biogenesis of Hherisomes is stimulated by Hh overexpression, they could have a degradative function to clear the excess of Hh. However, two arguments suggest otherwise. As shown above, Hherisomes are morphologically distinct from MVBs and are functionally different from lysosomes. Second, if Hherisomes were degradative, the density of Hh therein would be lower than in MVBs as Hh would not be protected from degradation and should not be detected. However, this is not what we observed. The density of Hh in Hherisomes is 5- to 10-fold higher than in MVBs (Table 1, line 5).

To confirm that Hherisomes are not degradative, we first assessed whether endogenous Hh undergoes any significant degradation. To do so, wild-type discs were incubated *ex vivo* with bafilomycin, an inhibitor of lysosome V-ATPase that results in a lysosomal neutral pH detrimental for protein degradation. This did not result in an increase in Hh immunofluorescence signal, neither in the posterior compartment nor in distal anterior cells (Fig. S3). However, this treatment resulted only in a strong increase of Hh in the first anterior cells at the A/P border. This is expected as, in these cells, Hh complexed with its receptor Ptc has been shown to undergo degradation (Callejo et al., 2006; Denef et al., 2000), thus providing a positive control.

To strengthen this result, we assessed the level of endogenous Hh in the posterior compartment in which *deep orange* (*dor*) was depleted. *dor* encodes for Vps18, a subunit of the HOPS and CORVET complexes that mediate the fusion of late endosomes with lysosomes where their degradation takes place (Sriram et al., 2003; van der Beek et al., 2019). However, *dor* RNAi did not lead to a significant increase in Hh staining, including in degradative compartments marked with poly-Ubi epitopes, suggesting that endogenous Hh is not readily degraded (Fig. S4). This is in agreement with the unchanged Hh staining in *dor* loss-of-function clones in the posterior compartment (D'Angelo et al., 2015).

We also considered the possibility that an excess of Hh production drives Hh to be degraded in Hherisomes. To address this, we repeated *dor* depletion on discs overexpressing Hh. We found that, as for endogenous Hh, overexpressed Hh was also not significantly degraded (Fig. S5). Taken together, these results strongly indicate that Hherisomes are not a degradative compartment and do not correspond to lysosomes.

Hh recruitment in Hherisomes is boosted by Rab11 activity

Examining the morphology of Hherisomes more closely, we noticed that a proportion of them appeared to be tubular (Fig. 4A) and that they are often grouped around vacuolar MVBs (Fig. 3A,B). This morphology is reminiscent of mammalian recycling tubules emanating from either early (fast) or recycling (slow) endosomes (van der Beek et al., 2019). Such tubules contain materials to be recycled back to the plasma membrane, consistent with their non-degradative function.

Journal of Cell Science (2021) 134, jcs258603. doi:10.1242/jcs.258603

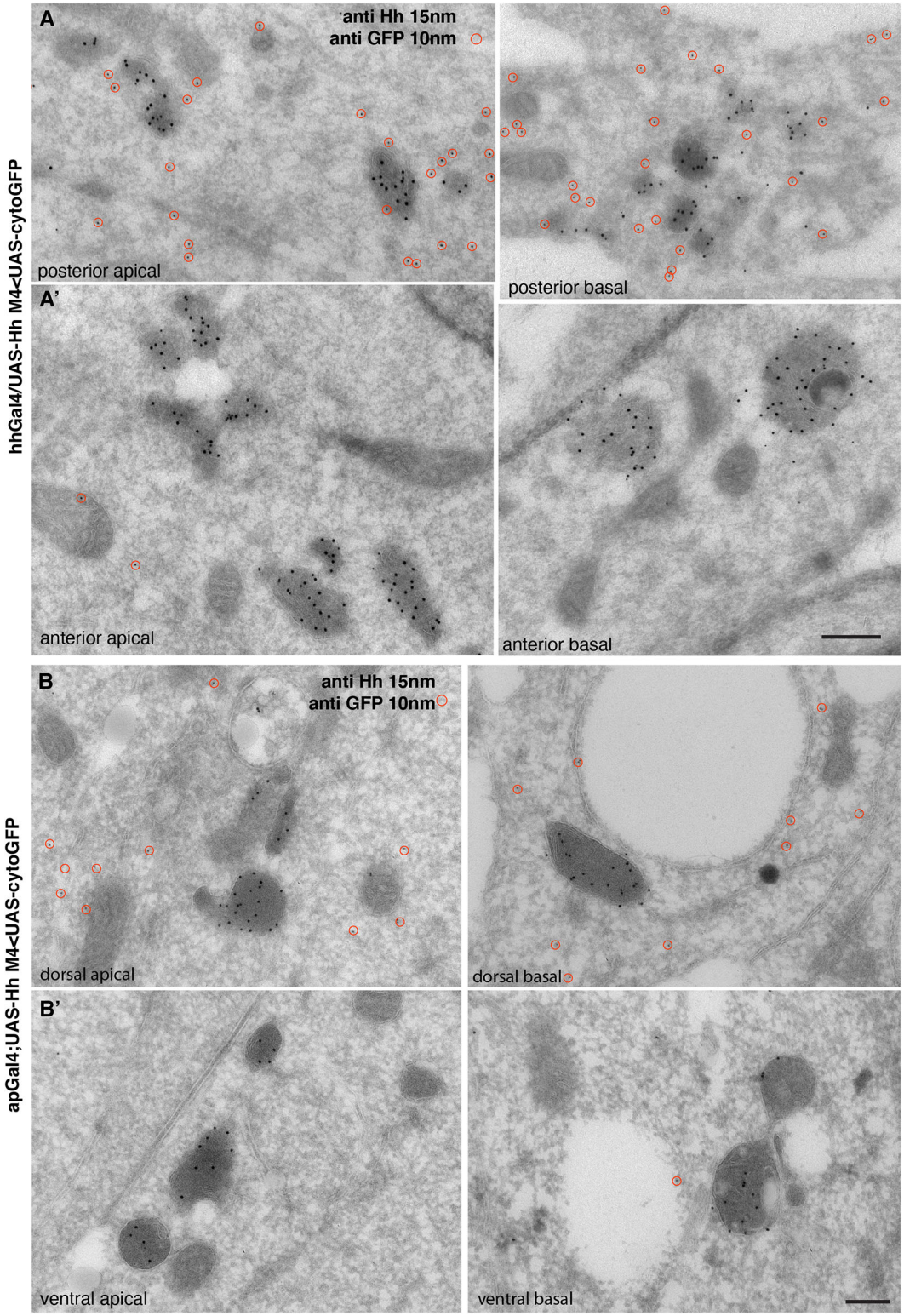

Fig. 2. Hherisomes are also present in the anterior compartment. (A,A′) Immunolocalisation of posteriorly overexpressed Hh in Hherisomes at the apical and basal side of the posterior cells (marked by cytoplasmic GFP; 10 nm PAG, red circles, A), and of the anterior cells (absence of GFP, A′). Hherisomes are present in both posterior and anterior compartments, ruling out that they are part of the biosynthetic pathway of the posterior cells. (B,B′) Immunolocalisation of dorsally overexpressed Hh in Hherisomes at the apical and basal side of dorsal cells [marked by cytoplasmic GFP, red circles (B); and ventral cells (absence of GFP, B′)]. Scale bars: 200 nm.

To test whether Hherisomes correspond to recycling tubules depending on Rab11 (Delevoye et al., 2014; Mattila et al., 2014), we first aimed to block slow recycling by expressing, together with Hh in the posterior compartment, a dominant-negative version of Rab11, YFP-Rab11S25N, that is deficient in GTP binding (Wang et al., 2000). Unfortunately, this led to animal lethality precluding

Journal of Cell Science (2021) 134, jcs258603. doi:10.1242/jcs.258603

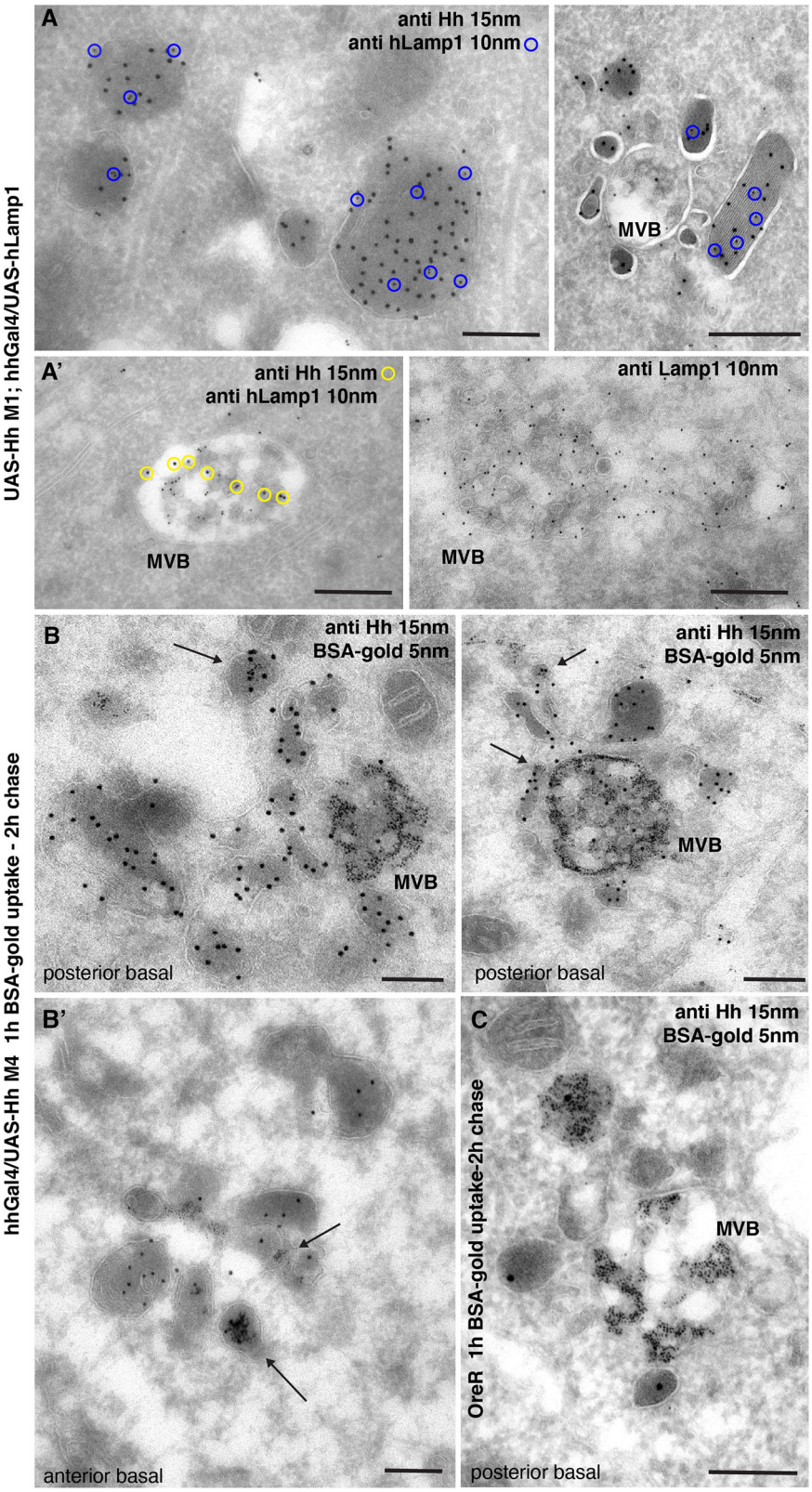

Fig. 3. Hherisomes are part of the endocytic pathway but distinct from MVBs. (A,A′) Immunolocalisation of posteriorly overexpressed Hh and hLamp1-HRP (10 nm PAG) in Hherisomes and MVBs. hLamp1 is marked with blue circles in A, and Hh is marked with yellow circles in A′. Both Hherisomes and MVBs are positive for Hh, but the density of hLamp1 is much higher in MVBs (A′) than in Hherisomes (A). (B,B′) Endocytosed BSA-gold, (5 nm) and posteriorly overexpressed Hh in MVBs and Hherisomes at the basal side of posterior (B) and anterior (B′) cells. Black arrows point to weakly BSA-gold-positive Hherisomes, but most of the Hherisomes are BSA-gold negative. (C) Endocytosed BSA-gold and endogenous Hh in MVBs and Hherisomes at the basal side of posterior disc cells in wild type (OreR). Scale bars: 200 nm.

this analysis (even with low expression of the Rab11 variant, data not shown). We then performed the converse experiment of overexpressing wild-type Rab11 (tagged with YFP) in the posterior compartment together with Hh. When compared to Hh overexpression alone, overexpression of Rab11-YFP led to a significant increase of Hh labeling density in the Hherisomes (Fig. 4B, Table 1, compare line 6 to line 5). Their size was also slightly larger, reaching up to 1 µm in some cases. Their number also slightly increased, especially in the anterior disc compartment (Table S3). These results show that Rab11 gain of function has a slight effect on Hherisome biogenesis, but a strong impact on the recruitment of Hh into Hherisomes.

Journal of Cell Science (2021) 134, jcs258603. doi:10.1242/jcs.258603

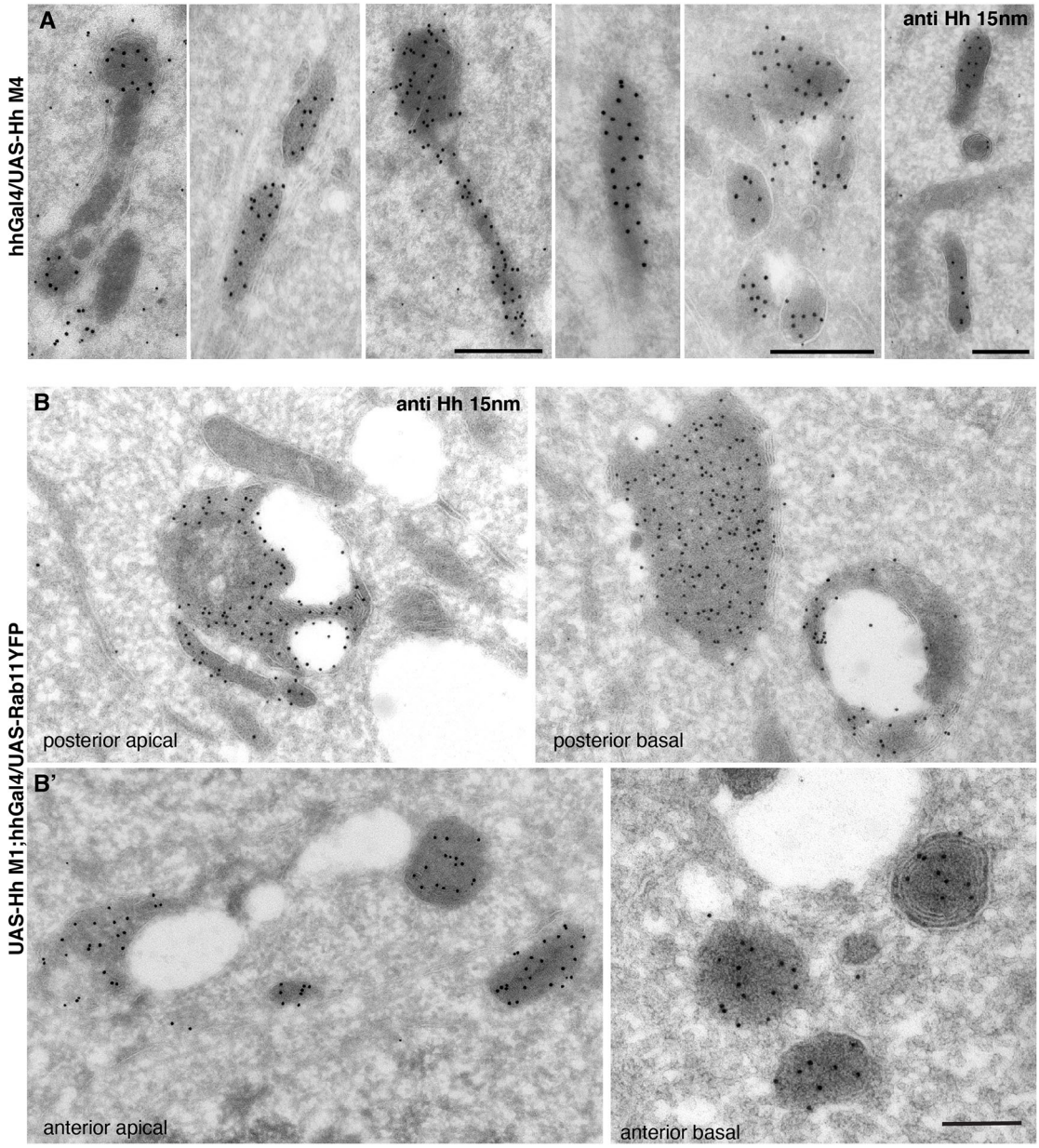

Fig. 4. Hherisome formation is boosted by Rab11 overexpression. (A) Gallery of tubular Hherisomes. (B,B′) Immunolocalisation of Hh in posterior (B) and anterior (B′) cells upon Rab11-YFP and Hh posterior co-overexpression. The size and Hh density of Hherisomes is increased upon joint Rab11 and Hh overexpression when compared to Hh alone (Figs 2, 3). Scale bars: 200 nm.

This indicates that Hherisomes may represent recycling tubular endosomes on which Hh loading is stimulated by Rab11 overexpression. This is consistent with the Rab11 functional link to recycling endosomes (Ren et al., 1998; Ullrich et al., 1996). Interestingly, the increase of Hh density in Hherisomes was also observed in the anterior compartment that overexpresses neither Hh nor Rab11 (Fig. 4B′, Table 1, compare line 6 to line 5).

In conclusion, Hherisomes are part of the endocytic pathway but are not MVBs and are not degradative lysosomes. Our results indicate that Hherisomes are Hh^{+} recycling tubules emanating from sorting endosomes (thus incorporating a bit of Lamp1 and BSA-gold).

Disp overexpression prevents Hherisome formation

To investigate the possible link between Hherisome formation and Hh patterning activity, we analysed the contribution of Disp (a positive regulator of Hh secretion) to Hherisome formation. In the wing disc, the patterning activity of Hh can be evidenced by the expression of target genes that have a function that is ultimately important for wing patterning. This is achieved by Hh activity that directly triggers different target gene expression. The high signaling level of Hh in the first row of anterior cells abbuting the A/P border activates expression of the transcription factor *engrailed* (*en*) and the Hh receptor *ptc*, whereas its low signaling level in anterior cells more distal to the A/P border activates expression of *dpp*. Therefore, the high-level signaling relates to the short-range activity of Hh, whereas the low-level signaling relates to its long-range activity.

In absence of Disp, Hh long-range activity is severely diminished and, consequently, Hh-dependent low signaling and growth are strongly affected (Burke et al., 1999). Disp has been shown to bind Hh once it reaches the plasma membrane and participates in its extraction

Journal of Cell Science (2021) 134, jcs258603. doi:10.1242/jcs.258603

from the plasma membrane to allow its spreading (Petrov et al., 2020; Tukachinsky et al., 2012). This function of Disp is supported by our data, as well showing that the level of Hh at the plasma membrane is lower in discs overexpressing Disp than in control (Fig. S6A-B′). Accordingly, the main localisation of overexpressed Disp is at the plasma membrane, both apical and basolateral (Fig. S6C; D'Angelo et al., 2015), at least when overexpressed.

We then tested the role of Disp in Hherisome formation. In the *disp* mutant, Hherisomes were clearly present, whether containing either endogenous (Fig. 5A) or overexpressed Hh (Fig. 5A′, Table 1, compare line 7 to 5), both at the apical and basal side. These results show that the Hh endocytosis mediating Hherisome formation is largely independent of Disp function.

Conversely, the overexpression of Disp together with Hh in the wing disc posterior compartment led to a severely reduced number of Hherisomes (93% reduction, Table S3), and the very few remaining are less densely labeled (Fig. 5B). In other words, the Hherisomes that are normally observed upon Hh overexpression were largely absent when Disp was also overexpressed. At the anterior compartment where Disp is not overexpressed, Hherisomes were present, albeit in lower numbers and less labeled (Fig. 5B′, Table 1, compare line 4 to line 2). This suggests that Disp overexpression in Hh-secreting posterior cells strongly interferes with Hherisome formation.

In conclusion, Hherisomes disappear upon Disp overexpression, whereas their loading in Hh is boosted upon Rab11 overexpression.

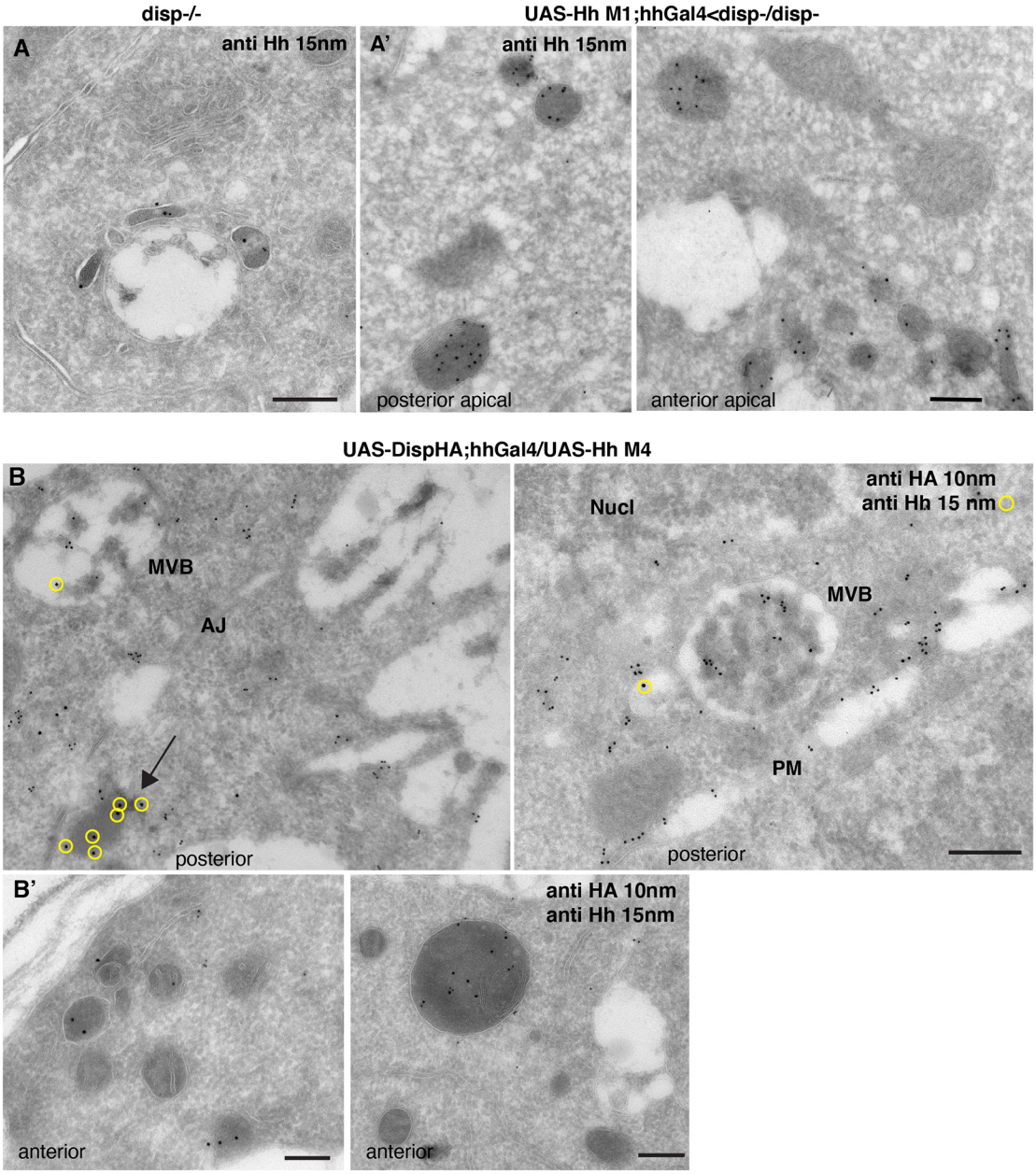

Fig. 5. Disp overexpression inhibits Hherisome formation. (A,A′) Immunolocalisation of endogenous Hh (A) and posteriorly overexpressed Hh (A′) in *disp*$^{-/-}$ mutant wing discs. (B,B′) Immunolocalisation of Hh in posterior (B) and anterior (B′) cells upon DispHA (10 nm PAG) and Hh posterior co-overexpression. Hherisomes and Hh (yellow circles) can barely be observed in posterior cells, except in the very few Hherisomes (black arrow), whereas Hherisomes form in anterior cells. AJ, apical junction; Nucl, nucleus; PM, plasma membrane. Scale bars: 200 nm.

Journal of Cell Science (2021) 134, jcs258603. doi:10.1242/jcs.258603

This makes these two conditions appropriate to test the function of Hherisomes in Hh activity.

Rab11 overexpression promotes high-level Hh signaling, whereas Disp overexpression decreases it

To test the role of Hherisomes in wing disc development, we used the potential of Disp and Rab11 overexpression in the Hh-producing cells to modulate Hherisome formation, and analysed the consequence on Hh signaling in the anterior compartment.

To do so, we measured the intensity and extension of *dpp* (low-level target) and En (high-level target) expression at the anterior side of the A/P margin (see Materials and Methods). In wild-type discs, *dpp* was typically expressed in anterior cells in a 7-8-cell stripe (Fig. 6A,D,E; Fig. S7), but its expression was low in the first 2-3 rows of anterior cells at the A/P border. This is because a high level of Hh signaling triggers expression of En, a direct repressor of *dpp* (Raftery et al., 1991; Sanicola et al., 1995). Accordingly, En was strongly expressed in the first 2-3 rows of anterior cells (Fig. 6A,A′).

Using this background, we measured the potential of Disp and Rab11 posterior overexpression to modify the width of the *dpp* and En expression domains. When compared to control, posterior Disp overexpression led to a decrease in En expression at the A/P border, consistent with a decrease of high Hh signaling level (Fig. 6B,B′, quantification in Fig. 6F; Fig. S7). Consequently, the *dpp* expression domain was broader, and *dpp*-expressing cells could be observed directly apposed to the posterior cells (Fig. 6B,B′,D,F; Fig. S8).

Conversely, posterior Rab11 overexpression increased the intensity level of En expression by 35% in the anterior cells (after normalisation to posterior En level; Fig. 6C,C′,F; Figs S7, S8). Accordingly, *dpp-lacZ* expression was reduced in the region close to the A/P border where En is strongly expressed, consistent with an increase in Hh signaling level (Fig. 6C,C′,E,F; Fig. S8).

As *dpp* and En expression depend on Hh signaling activity via its receptor Ptc, we then used immunofluorescence to assess the amount of Hh/Ptc complexes in the anterior cells at the A/P border. In the first anterior cells that receive a high level of Hh, the ligand-receptor complex could be visualised after internalisation by the formation of punctae positive for both Hh and Ptc (Fig. 6G; Gallet et al., 2008). We found that Rab11 posterior overexpression increased the number of Ptc/Hh punctae, consistent with an increase in signaling in cells close to the A/P, whereas Disp overexpression decreased it (Fig. 6G), in line with decreased signaling in these cells.

Taken together, these results show that Disp overexpression decreases the activity level of high (short range) Hh signaling pathway. Conversely, Rab11 overexpression leads to an increase in Hh signaling close to the A/P border and in the formation of the ligand/receptor Hh/Ptc complexes. Given that 90% of intracellular Hh is present in Hherisomes, and Hherisome formation is inhibited by Disp and stimulated by Rab11 posterior-specific overexpression, we propose that preventing Hherisome formation leads to a pool of Hh that is overall less potent for high signaling activity. Conversely, boosting Hherisome loading leads to a pool of Hh that is more competent for high-level signaling.

Posterior Rab11 overexpression leads to a stimulation of disc pouch growth in an Hh-dependent manner

Strikingly, we noticed that Rab11 and Disp overexpression leads to wing disc pouches of very different sizes. Indeed, the overexpression of Rab11 significantly increases the overall size of the disc pouch by 18% (Fig. 7A-B″,E), whereas Disp overexpression leads to a decrease in the pouch size by 14% (Fig. 7A-A″,C-C″,E). Thus, preventing Hherisome formation (through Disp overexpression) is associated with less pouch growth, whereas boosting Hherisome formation (through Rab11 overexpression) leads to increased pouch growth.

To show that the effect of posterior-specific Rab11 and Disp expression on overall pouch growth depends on Hh (and not on other factors), we overexpressed Rab11 and Disp in discs that were nearly *hh* null (homozygote hh^{ts2} mutants raised at a non-permissive temperature; Fig. 7D-D″). These discs were tiny and displayed a very small pouch when compared to wild-type discs (compare Fig. 7F and Fig. 7E). In this background, neither Rab11 nor Disp overexpression changes the pouch size, demonstrating that the Rab11 and Disp growth effect depends on the presence of Hh (Fig. 7D-D″,F).

Altogether, our results suggest that Hh-dependent signaling and growth are coupled, and are differentially regulated by Rab11 and Disp. Rab11 overexpression stimulates signaling in terms of both En and Hh/Ptc complex levels and pouch growth, whereas Disp overexpression reduces both.

Rab11 overexpression partially rescues the disc pouch growth of the *disp* mutant

The opposite effect of Rab11 and Disp overexpression on signaling and growth suggests the existence of two pathways, one through Hherisome formation boosted by Rab11, and the second that prevents Hherisome formation by Disp (see above). To understand how these two pathways intersect (whether they act in parallel or compete), we examined whether Rab11 is still able to induce growth in the absence of Disp activity.

In absence of Disp, Hh long-range activity is severely diminished and consequently, Hh-dependent signaling and growth are strongly affected (Burke et al., 1999). Indeed, as expected, the quantitative examination of *disp* mutant discs showed a 4-fold reduction in the number of Hh-responding cells in the anterior compartment, with a very thin stripe of *dpp* expression (two cells instead of seven or eight in wild-type discs) (compare Fig. 7A′ and Fig. 7G; Fig. S7). In addition, the pouch size of the *disp* mutant was significantly smaller (about 2.5-fold) than those of wild-type discs (compare Fig. 7E and Fig. 7I). Strikingly, Rab11 overexpression in *disp* mutant led to a strong increase (44%) of the disc pouch compared to *disp* mutant (compare Fig. 7G,G′ and Fig. 7H,H′, quantified in Fig. 7I). Note, however, that it did not reach the size of wild-type discs. The effect of Rab11 overexpression is therefore more potent when Disp is absent [compare the increase in pouch size in wild-type discs (18%) and in *disp* mutant discs (44%) (Fig. 7E,I)]. Altogether, our data suggest that Rab11 and Disp compete for Hh within posterior producing cells, raising the possibility of two co-existing (and competing) Hh trafficking routes.

DISCUSSION

In this study, we have identified intracellular recycling tubules that are specifically enriched in Hh and that have not previously been described in either fly or mammalian systems. We name these ‘Hh specialized recycling tubular endosomes’ Hherisomes. We propose that Hherisomes are dedicated to generating a pool of Hh with high potential signaling.

This study provides three main conceptual advances. First, we identify and characterise a new intracellular compartment, the Hherisome, that contains a high proportion of intracellular Hh (over 90% in a condition in which the expression of Hh is increased; Table 1). We show that Hherisomes represent recycling tubules emanating from endosomes. The formation of these tubules is

Journal of Cell Science (2021) 134, jcs258603. doi:10.1242/jcs.258603

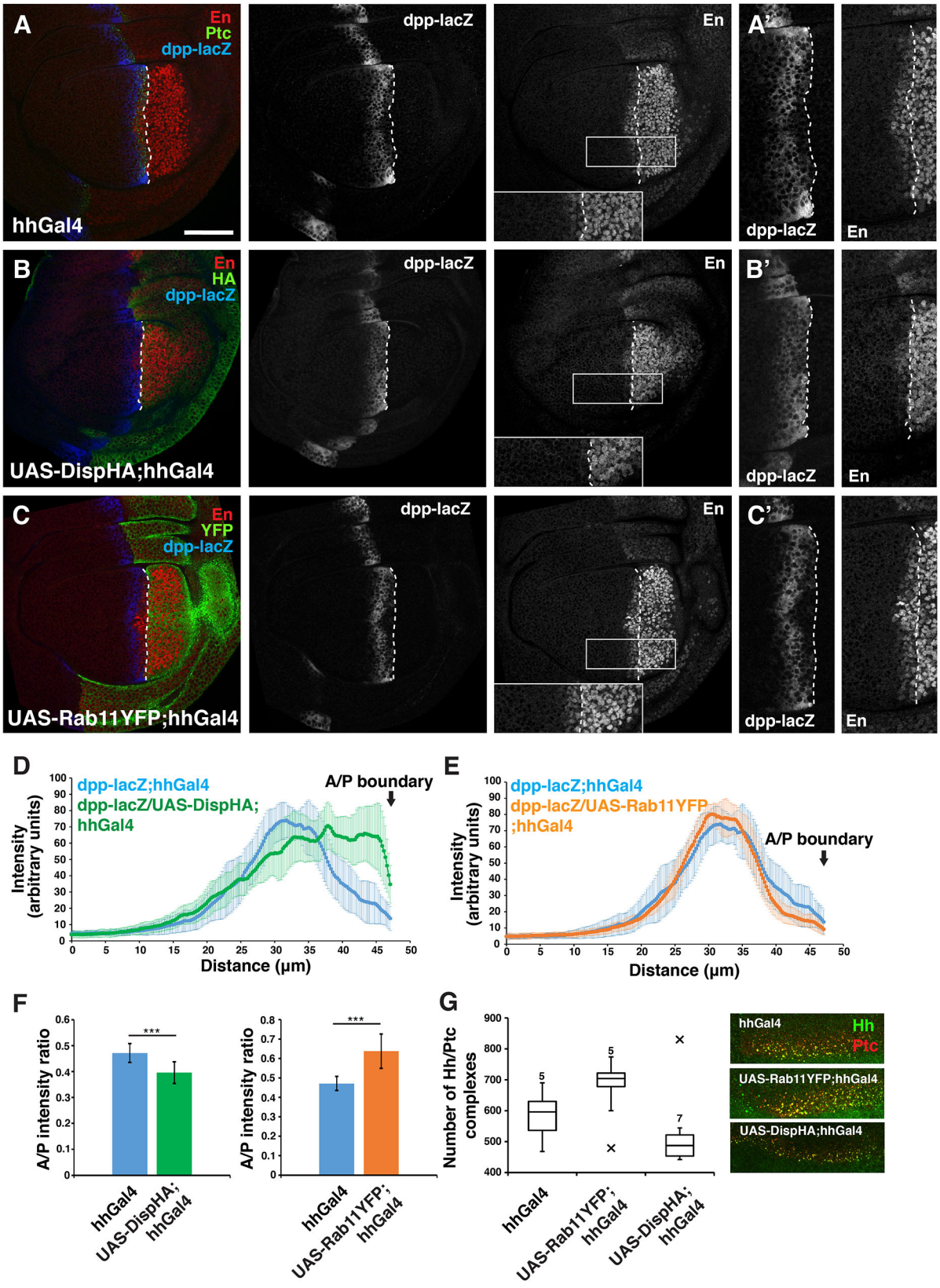

Fig. 6. See next page for legend.

largely promoted by full-length non-tagged dually lipidated Hh, and the loading of Hh in these structures is further triggered by Rab11 overexpression. Second, we show that Hh trafficking through Hherisomes modulates both Hh signaling and tissue growth. Indeed, promoting Hh loading in Hherisome through Rab11 overexpression enhances Hh signaling and the growth of the disc

Journal of Cell Science (2021) 134, jcs258603. doi:10.1242/jcs.258603

Fig. 6. Disp and Rab11 overexpression in Hh-producing cells leads to differential changes in Hh target gene expression patterns. (A-C′) En (red) and *dpp-lacZ* (blue) staining in wild type (A), Disp-overexpressing (B) and Rab11-overexpressing (C) wing discs. The A/P boundary (white dashed lines) is defined by Ptc in the control, and by YFP (for Rab11) or HA (Disp) immunostaining (green channels in the top row). Insets show the magnified squared area on the En channel. Close ups showing *dpp-lacZ* and En expression patterns are presented in A-C (A′,B′,C′). (D,E) Intensity plots of *dpp-lacZ* expression in wild type (blue, *n*=20), Disp overexpression (green, *n*=15) and Rab11 overexpression (orange, *n*=10). (F) Ratio of En immunofluorescence intensities between anterior and posterior cells in wild type (blue, *n*=11) compared to Disp overexpression (green, *n*=8, ***P=0.0011) and Rab11 overexpression (orange, *n*=10, ***P=0.0001). Data are mean±s.d. (G) Quantification of Hh/Ptc complexes in the anterior compartment in wild type compared to Disp overexpression (P=0.242) and Rab11 overexpression (P=0.16). The box represents the 25-75th percentiles, and the median is indicated. The whiskers show the 5-95th percentiles; x indicates outliers, which were included in the statistical analysis. Number of discs included in the quantification is indicated above the box plots. A representative image of each genotype is shown to the right (Hh, green; Ptc, red). *P*-values were calculated with two-tailed unpaired Student's *t*-tests. Scale bar: 50 µm (A-C).

pouch. Conversely, overexpressing Disp suppresses Hherisome formation, leading to a decrease in both signaling and growth. These findings suggest the existence of two competing Hh trafficking routes within posterior producing cells. Third, this provides further evidence for the coupling between Hh signaling and pouch size.

Why have Hherisomes never been observed before?

Ninety percent of intracellular Hh is found in Hherisomes; yet, to the best of our knowledge, Hherisomes have not been described before. Why not? The use of the detergents necessary to permeabilise the tissue (such as Triton X-100) to allow antibody penetration and visualisation by classical immunofluorescence may destroy the Hherisomes. The method used for performing the IEM described here only relies on fixing tissues with aldehydes followed by sectioning, thus exposing the epitopes without detergents. When IEM samples were subjected to detergent permeabilization, Hherisomes could no longer be observed (data not shown).

Tagging Hh with GFP would alleviate the need for tissue permeabilization. However, this does not completely recapitulate the dynamics and localisation of endogenous untagged Hh. Indeed, overexpressing HhGFP only leads to its modest incorporation into Hherisomes, contrary to what was observed with untagged Hh (Table S1).

Only full-length untagged Hh triggers Hherisome formation

We have shown that Hherisomes exist in wild-type disc and are not an artefact of Hh overexpression. In addition, only Hh overexpression leads to an increase in their number and size, and Hh density (Table S1), whereas overexpressing other molecules (such as Lamp1) that traffic through endosomes and could potentially saturate the system does not lead to a boost in Hherisome formation.

Hherisomes appear to be largely enriched in Hh (hence their name). Other molecules are also found in them, such as overexpressed Hh-N peptide fused with GFP at its C-terminus and SecGFP (Fig. S2B,C). However, these molecules are not enriched in Hherisomes, and they do not drive Hherisome biogenesis. Wg is not even present in these structures (Fig. S2A). So far, only the mature non-tagged Hh peptide that has a cholesterol moiety covalently attached to its C-terminus, and a palmitic acid (saturated fatty acid) on its N-terminus (Pepinsky et al., 1998; Porter et al., 1995) appears to be competent in boosting the formation of Hherisomes. Either this mature lipidated peptide associates to specific membrane domains that are hotspots for the endocytic events upstream of Hherisome formation, or it is more efficiently sorted into these recycling tubules once it reaches the vacuole of an endosome. However, Hh lipids and the hydrophobic interactions they might trigger with the lipid bilayer of endosomes are not the sole cause of this tubule biogenesis. Indeed, dually lipidated HhGFP does not trigger it (Table S1). Hh is therefore likely to have a specific property embedded in its tertiary conformation that allows this recruitment. This can be a result of its oligomerisation, interaction with different proteins, such as proteoglycans and lipid molecules, or further non-identified modifications.

Hherisomes are recycling tubular endosomes

Hherisomes are not intermediates of biosynthetic pathway transporting newly synthesised Hh to the plasma membrane because they are observed not only in the posterior disc cells that produce Hh, but also in the anterior cells that do not produce it. Instead, we propose that Hherisomes are recycling tubular endosomes, not part of the degradative endocytic compartments (late endosomes/MVBs and lysosomes), and this is for several reasons. First, Hherisomes are clearly morphologically different from MVBs, the electron-lucent vacuoles containing internal vesicles (as explained in Materials and Methods).

Second, if Hherisomes were lysosomes, they would strongly accumulate the fluid-phase endocytic marker BSA-gold after internalisation and long chase, and would be strongly positive for Lamp1, as lysosomes and MVBs do in mammalian cells (Sachse et al., 2002; Galmes et al., 2015). However, only 15% of Hherisomes are BSA-gold positive and when so, only weakly. Furthermore, they are largely negative for Lamp1. This makes Hherisomes unlikely to be lysosomes. Moreover, if Hherisomes were lysosomes, they would be degradative and Hh level would then increase when blocking the maturation of the degradative endosomal pathway through fusion of late endosomes to lysosomes. However, depletion of Dor, a subunit of the CORVET and HOPS complex that mediates this fusion, does not result in an increase in Hh level (by immunofluorescence). Furthermore, *ex vivo* treatment of wing disc with the proton pump inhibitor bafilomycin (that decreases the lysosomal pH and degradation) does not lead to an overall increase of Hh except in a few anterior cells, indicating that endogenous Hh is not significantly degraded in the posterior compartment and in the far anterior cells in which we have observed Hherisomes.

Third, Hherisomes can adopt an elongated/tubular shape and often appear grouped around the vacuole of an endosome (MVBs) that contains a small amount of Hh. Importantly, Hherisome loading of Hh is stimulated by Rab11 overexpression. Rab11 is reported not to trigger lysosome formation (Delevoye et al., 2014), but is linked to recycling endosomes (Ren et al., 1998; Ullrich et al., 1996). Therefore, we propose that Hherisomes are recycling tubules emanating from endosomal vacuoles.

The fact that the vast majority of intracellular Hh is observed in these recycling tubules (even in wild-type discs) suggests that Hh is stored (even transiently) in Hherisomes. A role for recycling tubules in storage has been suggested for the transporter Glut4 before release to the plasma membrane upon stimulation (Klip et al., 2019). Furthermore, the Birbeck granules (Mc Dermott et al., 2002) of Langherhans cells of the skin appear to specifically store the protein Langherin, and their biogenesis follows a route that is very similar to what we propose for Hherisomes.

As recycling tubules, we hypothesise that Hherisomes have the property to recycle their material to the plasma membrane, and as such, promote the release of Hh. Whether this recycling is constitutive or regulated is not presently known.

Journal of Cell Science (2021) 134, jcs258603. doi:10.1242/jcs.258603

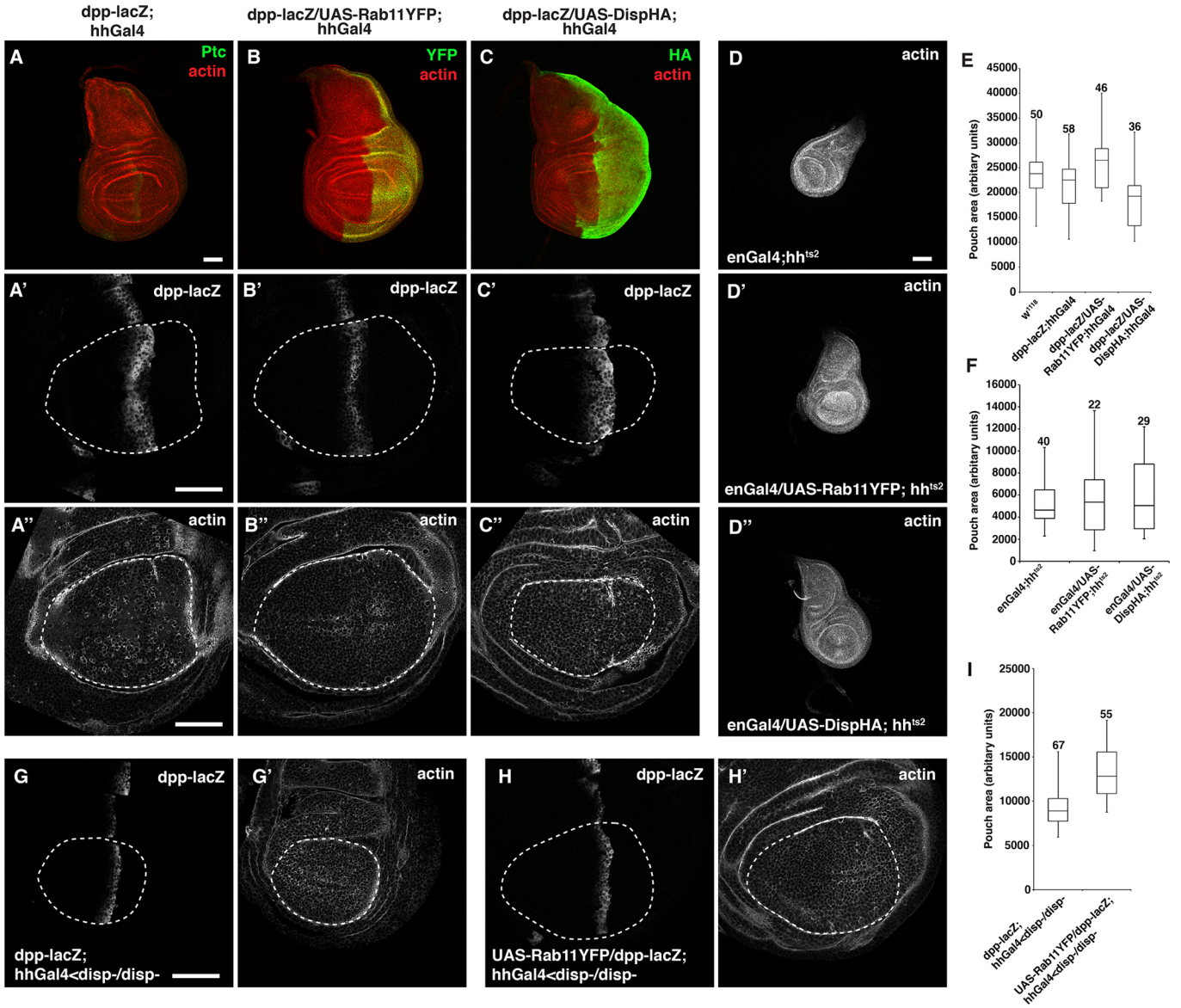

Fig. 7. Disp overexpression in Hh-producing cells leads to a decrease of wing pouch size, whereas Rab11 overexpression leads to an increase. (A-C) Representative images of imaginal discs from wild type (A), with posterior overexpression of Rab11-YFP (B), and of DispHA (C). The anterior-posterior boundary is defined by Ptc immunolabeling in the control (green in A), and YFP for Rab11 (green in B), or HA for Disp (green in C). Actin is labeled in red (A-C). (A′,B′,C′) *dpp-lacZ* expression in the same discs as in A-C (for quantification see Fig. 6). (A″-C″) Actin labeling in the aforementioned genotypes. The wing pouches are marked with white dashed lines. (D-D″) Representative images of hh^{ts2} homozygous mutant (D) and hh^{ts2} mutant discs expressing either Rab11 (D′) or Disp (D″) in the posterior cells. (E) Quantification of the wing pouch area. *P* value for *dpp-cyto-lacZ* (control) versus Rab11 overexpression, $P=9.98*10^{-5}$; *dpp-cyto-lacZ* (control) versus Disp overexpression, $P=0.0001$; w^{1118} (control) versus Rab11 overexpression, $P=0.0011$; w^{1118} (control) versus Disp overexpression, $P=1.842*10^{-6}$. (F) Quantification of the pouch area in the aforementioned hh^{ts2} genotypes. *P* values are the following: hh^{ts2} vs*Rab11;*hh^{ts2}, $P=0.4966$; hh^{ts2} vs*Disp;*hh^{ts2}, $P=0.5292$. (G-H′) Representative images of $disp^{-/-}$ homozygous mutant discs and $disp^{-/-}$ homozygous mutant discs overexpressing Rab11 in the posterior compartment. *dpp-lacZ* immunostaining (G,H) and filamentous actin labeling (G′,H′) of the same discs are shown. (I) Quantification of the wing pouch area. $P=6.9*10^{-15}$ for $disp^{-/-}$ (control) versus *Rab11;*$disp^{-/-}$. The box represents the 25-75th percentiles, and the median is indicated. The whiskers show the range. Sample numbers are above the box plots. Scale bars: 50 µm.

Model for Hherisome formation

Our model posits that upon secretion to the plasma membrane of the posterior cells, Hh is endocytosed. In this regard, Hh endocytosis at the apical side of the posterior cells has been shown previously (Callejo et al., 2011; D'Angelo et al., 2015). We propose that, following internalisation, Hh reaches endosomes (that are positive for Hh, albeit at a concentration 5-10 fold lower than Hherisomes), from which it is efficiently sorted in recycling tubules, the Hherisomes, in a Rab11-dependent manner, before being recycled.

Whether Hherisome formation depends on other Rabs remains to be tested. Earlier data (D'Angelo et al., 2015) suggested that a pool of Hh follows a rapid recycling route from early endosomes after its endocytosis through Rab4. As a result, we cannot formally exclude that Rab4 may have a modulating function in the formation of Hherisomes. However, D'Angelo et al. (2015) have shown that silencing Rab4 decreases Hh long-range/low-level signaling, but not short range. If the Rab4 pathway (fast recycling) were to be competing with the Rab11 pathway (slow recycling), the absence of Rab4 should lead to a pool of Hh more accessible to Rab11.

Journal of Cell Science (2021) 134, jcs258603. doi:10.1242/jcs.258603

Therefore, the overexpression of Rab11 should mimic a Rab4 loss-of-function phenotype. However, we show that Rab11 overexpression increases Hh short-range/high-level activity without a change in long range. Therefore, Rab4 likely works in parallel with Hherisome formation.

We also show that the endocytosis of dually lipidated non-tagged Hh upstream of Hherisome formation is largely independent of Disp, as Hherisomes form in an identical manner in wild type or *disp* mutant discs. It does not mean that Hh endocytosis is totally independent of Disp (Callejo et al., 2011; D'Angelo et al., 2015) but this endocytosis is not directly connected to Hherisome formation. Interestingly, though, Disp overexpression prevents the formation of Hherisomes.

The role of Hherisomes: increasing Hh signaling

Expressing Rab11 specifically in the posterior compartment increased the expression of the high threshold Hh target En, suggesting that stimulating Hherisome loading by Rab11 leads to more potent Hh signaling. Conversely, both Hherisome formation and high signaling level are inhibited by Disp overexpression in the posterior. Therefore, we propose that the prevention of Hherisome formation leads to reduced Hh signaling activity.

These data suggest that Hh exists in two pools, both available for signaling activity, but with distinct signaling capacities, likely due to different routes of Hh trafficking. We propose that the first pool of Hh is mediated by Disp, which extracts Hh from the plasma membrane, resulting in an Hh pool with a low signaling capacity that is visible with *dpp* expression. Indeed, the absence of Disp leads to the lack of low signaling capacity illustrated by a decrease in *dpp* expression (Burke et al., 1999). Conversely, when Disp is overexpressed, this pool of low Hh activity is predominant.

However, the expression of Hh target genes at the A/P border that require high Hh signaling, such as an increased level of Ptc, is still clearly visible in the first 1-2 anterior cells in the *disp* mutant (Burke et al., 1999; our observation). This shows that high Hh signaling depends on a second Disp-independent pool. This pool is formed through Hherisomes via Rab11.

How can Hherisomes form a pool of Hh endowed with high Hh signaling? We propose that in Hherisomes, Hh acquires specific properties that renders it more active in signaling. Alternatively, Hherisomes may lead to the further targeting of Hh to different routes that have been proposed. One, transcytosis of Hh from the apical to the basal side of producing cells could be responsible for the activation of high Hh signaling target, such as Ptc expression (Callejo et al., 2011). Hherisomes could mediate this transcytosis. Second, the activation of Ptc (but not the low-level signaling target *dpp*) has been shown to be dependent on cytonemes, which are long cellular extensions that connect Hh-secreting to Hh-receiving cells (Bischoff et al., 2013; Chen et al., 2017; González-Méndez et al., 2017). Cytonemes have only been observed at the basal side, but it is possible that apical Hherisomes move to the basal side and promote the loading of Hh on these cytonemes. Last, Hh has been shown to be associated/present in lipoprotein particles. This association could have taken place within Hherisomes, especially considering that only fully lipidated Hh is efficiently sorted. However, lipoproteins have been associated with the low-level signaling of Hh, and are therefore unlikely to be related to Hherisomes. Altogether, the link of Hherisomes to pre-existing models remains to be further investigated as our present study was not designed to test pre-existing models of Hh trafficking and signaling.

In conclusion, we propose that the pool of Hh that is endocytosed and recycled through Hherisomes has different properties than the pool of Hh that has not been trafficked through Hherisomes. One of these properties triggers higher signaling and also pouch growth (see below).

Hherisomes are coupled to pouch growth

Hh trafficking through Hherisomes – stimulated by Rab11 – not only displays a high signaling activity, but also stimulates pouch growth. Furthermore, this increase in pouch growth depends on Hh; Rab11 overexpression is not sufficient to rescue the pouch growth of the tiny wing pouches found in conditional null (hh^{ts2}/hh^{ts2}) discs. This shows that the pouch growth promoted by Rab11 overexpression likely depends on Hherisome formation.

It is important to note that in all of the experiments in which Rab11 is overexpressed in the posterior compartment, the effect on growth is only observed on the pouch size, not the whole disc (data not shown). This indicates that pouch growth requires a posterior-specific non-cell autonomous secreted factor that depends on Rab11. We propose that this factor is Hh. It is possible that the activity of Dpp, a regulator of wing disc tissue growth (Barrio and Milán, 2017; Bosch et al., 2017; Matsuda and Affolter, 2017) is also affected. As Dpp expression and signaling is regulated by Hh, we cannot rule out the possibility that the manipulation of Rab11 expression affects Dpp signaling directly, not through Hherisome formation and Hh signaling. The relationship between pouch growth, Dpp and Hherisomes will need to be further investigated.

Rab11- and Disp-mediated pathways compete for Hh

In our model, Rab11 and Disp pathways appear to compete for Hh. Rab11 promotes Hherisome formation after Hh endocytosis, whereas Disp extracts Hh from the plasma membrane. Our data suggest that the Rab11-dependent step is limited in the wild-type context. This limitation is illustrated by the effect of Rab11 overexpression, which is able to further increase the formation of, and Hh loading in, Hherisomes (Fig. 4) compared to Hh overexpression alone. It also explains why Rab11 overexpression is more potent in pouch growth when Disp is absent, with an increase of 44% of pouch size in the absence of Disp when compared to 18% of increase in the presence of Disp (Fig. 7). The molecular details by which these two routes intersect will need to be further investigated.

In conclusion, although the mechanism of action of morphogens in tissue organization during development has been highly studied, our knowledge of how cells exchange information through morphogens is still preliminary, and the models are highly debated. More specifically, very little is known about the intracellular route taken by lipidated Hh, the cellular machinery required for its secretion, and how it is transported in order to act as a morphogen. The identification of Hherisomes opens new avenues in our understanding of how morphogen signals are exchanged between cells, and will likely help more generally in our understanding of the mechanisms of cell-cell interaction.

MATERIALS AND METHODS

Fly stocks and *Drosophila* genetics

Flies were raised on standard cornmeal-agar medium. For IEM experiments, all crosses were performed at 25°C using the following fly lines: OreR, UAS-secGFP (Chu et al., 2006), hhGal4 (Tanimoto et al., 2000), dppGal4 [Bloomington *Drosophila* Stock Center (BDSC,1553)], apGal4 (BDSC, 3041), UAS-Wg^{HA} (Franch-Marro et al., 2008), UAS-$Disp^{HA}$ (Burke et al., 1999, BDSC, 55076), UAS-Hh (M1) and UAS-Hh (M4) (full-length non-tagged, dually lipidated form, Ingham and Fietz, 1995), UAS-hLamp1-Hrp (Lloyd et al., 2002), UAS-HhN-GFP (Gorfinkiel et al., 2005), UAS-HhGFP (full-length tagged dually lipidated form, Torroja et al., 2004), UAS-cytoGFP (BDSC, 1521, for chromosome II, and BDSC, 1522, for

chromosome III), UAS-Rab11-YFP (BDSC, 50782), *disp*^{SO37707} (Burke et al., 1999) and UAS-Ptc^{1130X} (Johnson et al., 2000). Maternal and paternal genotypes, as well as final genotypes, are detailed in Table S4.

To induce Hh expression in the posterior compartment, two different transgenes, UAS HhM4 and UAS HhM1, were expressed under the control of *hh* own promoter (*hhGal4*). To induce *dor* loss of function, both in wild-type and *hh* gain-of-function background, five males of *UAS-dor* RNAi [Vienna *Drosophila* Resource Center (VDRC), 107053] were crossed to 15 *w*^{1118}*; tubGal80*^{ts}*<dpp-lacZ; hhGal4/TM6b,Tb* or *w*^{1118}*; tubGal80*^{ts}*; hhGal4<UAS-Hh(M4)/TM6b,Tb* virgins. Crosses were kept in vials at 25°C, and parents were transferred every 8 h to new medium. Vials with embryos were transferred to 18°C for 48 h, and then larvae were shifted to 29°C for 72 h before dissection. As a neutral UAS control we used *UAS-Ci* RNAi (VDRC, 100620).

To overexpress Disp^{HA} or Rab11-YFP in wild-type background, five males of *UAS-Disp*^{HA} (BDSC, 55076) and *UAS-Rab11-YFP* (BDSC, 50782) were crossed to 15 *tubGal80*^{ts}*<dpp-lacZ; hhGal4/TM6b,Tb* virgins. Crosses were kept in vials at 25°C, and parents were transferred every 8 h to new medium. Vials with embryos were transferred to 18°C for 48 h, and then larvae were shifted to 29°C for 72 h before dissection. As controls, we crossed *w*^{1118}/Y males to *w*^{1118}*;tubGal80*^{ts}*<dpp-lacZ; hhGal4/TM6b,Tb* virgins at the same time.

To generate a conditional *hh* null context, ten males of *UAS-Disp*^{HA}*;hh*^{ts2}*/SM6-TM6b* and *UAS-Rab11-YFP; hh*^{ts2}*/SM6-TM6b* were crossed to 50 *w*^{1118}*; enGal4<tubGal80*^{ts}*; hh*^{ts2}*/SM6-TM6b* virgins. Crosses were kept in bottles at 18°C, and parents were transferred every 12 h to new medium. Vials with embryos were kept at 18°C for 168 h, and then larvae were shifted to 29°C for 48 h before dissection. As controls, we crossed *w*^{1118}*/Y;hh*^{ts2}*/TM6b,Tb* males to *w*^{1118}*; enGal4<tubGal80*^{ts}*; hh*^{ts2}*/SM6-TM6b* virgins at the same time. Inactivation for 48 h at restrictive temperature causes pupal lethality of the *hh*^{ts2} homozygotes with 100% penetrance in early pupal stages.

To overexpress Rab11-YFP in Hh-secreting cells in a *disp*^{SO37707} (Burke et al., 1999) mutant background, five *w*^{1118}*/Y; UAS-Rab11-YFP; disp*^{SO37707}*/SM6-TM6b* males were crossed to 15 *w*^{1118}*; tubGal80*^{ts}*<dpp-lacZ; hhGal4<disp*^{SO37707}*/TM6b,Tb* virgins. Crosses were kept in vials at 25°C, and parents were transferred every 8 h to new medium. Vials with embryos were kept at 25°C for 24 h, and then larvae were shifted to 29°C for 72 h before dissection.

Because of the natural variation in disc growth, we aimed to analyse at least 20 discs/genotype/biological replicate, but we did not define an upper threshold for maximum sample number. We aimed for the maximum technically doable disc number (in other words, the most possible simultaneous dissections within fixation batches). Each experiment for wing disc growth (Fig. 7E-I) was carried out with two biological replicates. We did not exclude any outliers from any of the statistical tests.

Within each biological replicate, three technical replicates were used (three independent cross/genotype). For Hh target gene expression analysis, discs from the second aforementioned biological replicate were selected for intensity measurements (Fig. 6D-G; Fig. 7I).

Immunoelectron microscopy

Wing discs were dissected from third instar wandering larvae and fixed in 2% paraformaldehyde (PFA) and 0.2% glutaraldehyde in 0.1 M phosphate buffer (pH 7.4), for 2-3 h at room temperature, followed by overnight incubation at 4°C in 1% PFA in phosphate buffer, and stored in 1% PFA in phosphate buffer at 4°C. Discs were very lightly stained with 1% Toluidine Blue and individually embedded in 15% gelatin (Liou et al., 1996) in such a way that sections as presented in Fig. S1A can be generated. Thick frozen sections (60-80 nm) were incubated with antibodies described below (Slot and Geuze, 2007). Rabbit antibodies were recognized by protein A conjugated to 10 or 15 nm gold particles (protein A gold, PAG). Mouse antibodies were detected by a rabbit anti-mouse IgG (DakoCytomation Denmark A/S, Glostrup, Denmark, 1:50) or rabbit anti-mouse IgG (Rockland, 1:250) followed by PAG. Double labeling procedures were performed sequentially as described by Slot and Geuze (2007).

A note of definition: we used the term MVBs to refer to the large vacuolar structures (0.5-1 µm in diameter) observed at the ultrastructural level in disc cells that contain over five internal vesicles. Those located at the basal side are efficiently reached by endocytosed BSA-gold where it is applied, and they all are heavily positive for overexpressed Lamp1. Importantly, we did not observe early endosomes (large electron-lucent vacuoles with none to few internal vesicles) or lysosomes (dark structures containing degraded materials and remnants of organelles). Therefore, the observed MVBs, although morphologically homogeneous, likely correspond to functionally different endosomes. Some cells display autophagosomes.

Immunofluorescence

Conventional staining was performed as described previously (Matusek et al., 2014). Fixed and immunostained wing imaginal discs were mounted in Vectashield mounting medium supplemented with DAPI (Vector Laboratories).

Antibodies

For IEM, we used the rabbit polyclonal anti-Hh antibody (a generous gift from Tom Kornberg, Cardiovascular Research Institute, University of California, San Francisco, San Francisco, CA; 1:500), mouse monoclonal anti-HA (clone 16B12, Covance, 1:300) and rabbit polyclonal anti-GFP (ab290, Abcam, 1:600). The rabbit polyclonal anti-hLamp1 931B (1:100) was a generous gift from Mitsunori Fukuda, Department of Developmental Biology and Neurosciences, Tohoku University, Sendai, Miyagi, Japan.

For immunofluorescence studies, we used the following primary antibodies: chicken polyclonal anti-β-gal (GeneTEX, GTX77365, 1:1000), mouse anti-GFP (Roche, 1814460, 1:100), mouse anti-Ptc (provided by Phil Ingham, LKC School of Medicine, Nanyang Technological University, Singapore; 1:400), affinity-purified rabbit anti-Hh (1:500, Matusek et al., 2014), mouse-anti-Ubi (clone FK2, ENZO Life Sciences, BML-PW8810-0100, 1:1000), guinea-pig anti-Engrailed (1:100; generated in this study, validated by immunofluorescence, subcellular-nuclear-distribution and endogenous expression pattern analysis; Fig. 6; Fig. S8). Fluorescent secondary antibodies used were as follows: Cy3- or Cy5-conjugated donkey anti-chicken IgG (1:200, Jackson ImmunoResearch Laboratories, 703-165-155, 703-175-155), goat anti-mouse IgG Alexa Fluor 488 (1:500, Life Technologies, A32723); donkey anti-mouse IgG Alexa Fluor 546 (1:500, Life Technologies, A10036), Cy3-conjugated anti-guinea pig IgG (1:200, Jackson ImmunoResearch Laboratories, 106-165-003), goat anti-rabbit Cy5 (1:200, Jackson ImmunoResearch Laboratories, 111-175-144) and rhodamine phalloidin (1:100, Sigma-Aldrich, P1951).

BSA-gold uptake

Dissected whole wing discs were incubated at room temperature in Schneider's medium containing 1% serum supplemented with BSA coupled to 5 nm gold for 1 or 2 h. They were then extensively rinsed and either fixed as above, or for the chase, further incubated at room temperature in Schneider's medium containing 10% serum for 2 to 4 h before rinsing and fixation. Importantly, because of the disc morphology, only the basal side of the epithelial disc cells was accessible to BSA gold. Consequently, only the basal endocytic compartments were reached. The quantification of the number of basal Hherisomes reached by BSA gold was (Table S2) achieved by counting all the Hherisomes present at the basal side of the epithelia. This was set at 100%.

Bafilomycin treatment

Dissected wing discs were incubated at room temperature in Schneider's medium containing 10% serum supplemented with 100 nM bafilomycin (Sigma-Aldrich, B1793) for 1 h. They were then rinsed in PBS and processed for immunofluorescent staining. As bafilomycin was dissolved in DMSO, control discs were incubated in Schneider's medium containing 10% serum and DMSO.

Quantification of electron micrographs

The quantification of the numbers of Hherisomes in Table S1 was performed by scoring disc sections in each background directly under the microscope. Cell profiles (144-484) were examined for their number of Hherisomes that were directly recorded as 'number of Hherisomes/cells'. All the data were added, hence the lack of s.e.m. Representative pictures are shown in Fig. 1B,B″ (arrows).

The quantification of the number of Hherisomes when Rab11 and Disp were co-expressed with Hh (Table S3) was performed by scoring the

number of Hherisomes per field (10 μm^2) where they were present (~70 such fields).

The labeling density (that corresponds to concentration) of Hh in Hherisomes and MVBs was calculated by counting the number of gold particles corresponding to Hh in organelle profiles divided by their surface area (that was estimated by point hit as described previously, Kondylis and Rabouille, 2003; Rabouille et al., 1999). This was carried out using a grid of 0.5 cm on pictures at 60 to 80 k. The number of Hherisomes counted per condition is indicated in the tables, and derives from multiple electron micrographs taken from duplicated or triplicated experiments. The percentage of Hherisomes positive for BSA-gold was estimated at the basal side only over the total number of Hherisomes.

The relative distribution represents the quantitative distribution of gold particles over different compartments. It is estimated by counting the total number of gold particles per micrographs (G_{total}) and assigning each gold particle to a specific compartment (G_{comp}). The ratio G_{comp}/G_{total} gives the relative distribution of gold particles over different cell compartments, such as 90% of Hh in Hherisomes (Rabouille et al., 1999).

Imaging and quantification in immunofluorescence studies

All confocal images were recorded using a Leica TCS SP5 confocal laser scanning microscope. To measure the pouch/wing discs size, images were collected using a 10× objective (HCX Plan Fluotar NA=0.3) without zoom at a 2048×2048 resolution with a speed of 400 Hz in a single plane. Wing pouches were outlined in the phalloidin channel, and measured using the Fiji 'polygon selections' tool. Hh/Ptc complexes were counted manually on images with a 1024×1024 resolution, and recorded using a 40× objective (HCX PLAN APO;NA=1.3) at 1.6× magnification with a speed of 400 Hz, within a 19 slice range (1 μm), slice by slice using the Fiji 'cell counter' plug-in. *dpp-lacZ* intensity was measured on single slices on images recorded at a resolution of 1024×1024, using a 40× objective (HCX PLAN APO;NA=1.3) at a 1.6× zoom level, with a speed of 400 Hz, within a 200×100 pixel rectangle. For En analysis, the same imaging conditions and a 100×100 pixel square was used. To calculate the anterior/posterior En intensity ratios, the total intensity of En staining was measured in a 50×50 pixel square in the anterior and in the posterior compartment using the 'measure' command in Fiji. All raw measurement data were transferred to, and treated, in Microsoft Excel 2016. To test for statistical significance, we applied a two-tailed unpaired Student's *t*-test.

Acknowledgements

We thank Tom Kornberg for the Hh antibody and Tanvi Gore for discussion and assistance. The IEM was performed at the Department of Cell Biology, UMC Utrecht, and at the Centre Commun de Microscopie Appliquée, Université Nice Côte d'Azur, Microscopy and Imaging platform Côte d'Azur (MICA) and we thank Sophie Pagnotta for technical support.

Competing interests

The authors declare no competing or financial interests.

Author contributions

Conceptualization: S.P., T.M., P.P.T., C.R.; Validation: S.P., T.M., B.H., P.P.T., C.R.; Formal analysis: S.P., T.M., B.H., C.R.; Investigation: S.P., T.M., B.H., C.R.; Resources: P.P.T., C.R.; Data curation: S.P., T.M., B.H., P.P.T., C.R.; Writing - original draft: S.P., T.M., P.P.T., C.R.; Writing - review & editing: S.P., T.M., P.P.T., C.R.; Visualization: S.P., T.M., B.H., C.R.; Supervision: P.P.T., C.R.; Project administration: P.P.T., C.R.; Funding acquisition: P.P.T., C.R.

Funding

This work was supported by the Ligue Nationale Contre le Cancer 'Equipe Labellisée 2016', Labex Signalife (ANR-11-LABX-0028-01) and the Agence Nationale de la Recherche (ANR-15-CE13-0002-01 and ANR-18-CE13-0003 to P.P.T.).

Peer review history

The peer review history is available online at https://journals.biologists.com/jcs/article-lookup/doi/10.1242/jcs.258603

References

Ayers, K. L., Gallet, A., Staccini-Lavenant, L. and Thérond, P. P. (2010). The long-range activity of Hedgehog is regulated in the apical extracellular space by the glypican Dally and the hydrolase Notum. *Dev. Cell* **18**, 605-620. doi:10.1016/j.devcel.2010.02.015

Barrio, L. and Milán, M. (2017). Boundary Dpp promotes growth of medial and lateral regions of the *Drosophila* wing. *eLife* **6**, e22013. doi:10.7554/eLife.22013

Basler, K. and Struhl, G. (1994). Compartment boundaries and the control of *Drosopfiffa* limb pattern by *Hedgehog* protein. *Nature* **368**, 208-214. doi:10.1038/368208a0

Bischoff, M., Gradilla, A.-C., Seijo, I., Andrés, G., Rodríguez-Navas, C., González-Méndez, L. and Guerrero, I. (2013). Cytonemes are required for the establishment of a normal Hedgehog morphogen gradient in *Drosophila* epithelia. *Nat. Cell Biol.* **15**, 1269-1281. doi:10.1038/ncb2856

Bosch, P. S., Ziukaite, R., Alexandre, C., Basler, K. and Vincent, J.-P. (2017). Dpp controls growth and patterning in *Drosophila* wing precursors through distinct modes of action. *eLife* **6**, e22546. doi:10.7554/eLife.22546

Brand, A. H. and Perrimon, N. (1993). Targeted gene expression as a means of altering cell fates and generating dominant phenotypes. *Development* **118**, 401-415.

Briscoe, J. and Thérond, P. P. (2013). The mechanisms of Hedgehog signalling and its roles in development and disease. *Nat. Rev. Mol. Cell Biol.* **14**, 416-429. doi:10.1038/nrm3598

Burke, R., Nellen, D., Bellotto, M., Hafen, E., Senti, K.-A., Dickson, B. J. and Basler, K. (1999). Dispatched, a novel sterol-sensing domain protein dedicated to the release of cholesterol-modified hedgehog from signaling cells. *Cell* **99**, 803-815. doi:10.1016/S0092-8674(00)81677-3

Callejo, A., Torroja, C., Quijada, L. and Guerrero, I. (2006). Hedgehog lipid modifications are required for Hedgehog stabilization in the extracellular matrix. *Development* **133**, 471-483. doi:10.1242/dev.02217

Callejo, A., Bilioni, A., Mollica, E., Gorfinkiel, N., Andrés, G., Ibáñez, C., Torroja, C., Doglio, L., Sierra, J. and Guerrero, I. (2011). Dispatched mediates Hedgehog basolateral release to form the long-range morphogenetic gradient in the *Drosophila* wing disk epithelium. *Proc. Natl. Acad. Sci. USA* **108**, 12591-12598. doi:10.1073/pnas.1106881108

Chen, W., Huang, H., Hatori, R. and Kornberg, T. B. (2017). Essential basal cytonemes take up Hedgehog in the *Drosophila* wing imaginal disc. *Development* **144**, 3134-3144. doi:10.1242/dev.149856

Chu, T., Chiu, M., Zhang, E. and Kunes, S. (2006). A C-terminal motif targets Hedgehog to axons, coordinating assembly of the *Drosophila* eye and brain. *Dev. Cell* **10**, 635-646. doi:10.1016/j.devcel.2006.03.003

D'Angelo, G., Matusek, T., Pizette, S. and Thérond, P. P. (2015). Endocytosis of Hedgehog through dispatched regulates long-range signaling. *Dev. Cell* **32**, 290-303. doi:10.1016/j.devcel.2014.12.004

Delevoye, C., Miserey-Lenkei, S., Montagnac, G., Gilles-Marsens, F., Paul-Gilloteaux, P., Giordano, F., Waharte, F., Marks, M. S., Goud, B. and Raposo, G. (2014). Recycling endosome tubule morphogenesis from sorting endosomes requires the kinesin motor KIF13A. *Cell Rep.* **6**, 445-454. doi:10.1016/j.celrep.2014.01.002

Denef, N., Neubüser, D., Perez, L. and Cohen, S. M. (2000). Hedgehog induces opposite changes in turnover and subcellular localization of patched and smoothened. *Cell* **102**, 521-531. doi:10.1016/S0092-8674(00)00056-8

Franch-Marro, X., Wendler, F., Griffith, J., Maurice, M. M. and Vincent, J.-P. (2008). In vivo role of lipid adducts on Wingless. *J. Cell Sci.* **121**, 1587-1592. doi:10.1242/jcs.015958

Gallet, A., Staccini-Lavenant, L. and Thérond, P. P. (2008). Cellular trafficking of the glypican Dally-like is required for full-strength Hedgehog signaling and wingless transcytosis. *Dev. Cell* **14**, 712-725. doi:10.1016/j.devcel.2008.03.001

Galmes, R., ten Brink, C., Oorschot, V., Veenendaal, T., Jonker, C., van der Sluijs, P. and Klumperman, J. (2015). Vps33B is required for delivery of endocytosed cargo to lysosomes. *Traffic* **16**, 1288-1305. doi:10.1111/tra.12334

González-Méndez, L., Seijo-Barandiarán, I. and Guerrero, I. (2017). Cytoneme-mediated cell-cell contacts for Hedgehog reception. *eLife* **6**, e24045. doi:10.7554/eLife.24045

Gorfinkiel, N., Sierra, J., Callejo, A., Ibañez, C. and Guerrero, I. (2005). The *Drosophila* ortholog of the human Wnt inhibitor factor shifted controls the diffusion of lipid-modified Hedgehog. *Dev. Cell* **8**, 241-253. doi:10.1016/j.devcel.2004.12.018

Gradilla, A.-C., González, E., Seijo, I., Andrés, G., Bischoff, M., González-Mendez, L., Sánchez, V., Callejo, A., Ibáñez, C., Guerra, M. et al. (2014). Exosomes as Hedgehog carriers in cytoneme-mediated transport and secretion. *Nat. Commun.* **5**, 5649. doi:10.1038/ncomms6649

Ingham, P. W. and Fietz, M. J. (1995). Quantitative effects of hedgehog and decapentaplegic activity on the patterning of the *Drosophila* wing. *Curr. Biol.* **5**, 432-440. doi:10.1016/S0960-9822(95)00084-4

Johnson, R. L., Milenkovic, L. and Scott, M. P. (2000). In vivo functions of the patched protein: requirement of the C terminus for target gene inactivation but not Hedgehog sequestration. *Mol. Cell* **6**, 467-478. doi:10.1016/S1097-2765(00)00045-9

Klip, A., McGraw, T. E. and James, D. E. (2019). Thirty sweet years of GLUT4. *J. Biol. Chem.* **294**, 11369-11381. doi:10.1074/jbc.REV119.008351

Kondylis, V. and Rabouille, C. (2003). A novel role for dp115 in the organization of tER sites in *Drosophila*. *J. Cell Biol.* **162**, 185-198. doi:10.1083/jcb.200301136

Liou, W., Geuze, H. J. and Slot, J. W. (1996). Improving structural integrity of cryosections for immunogold labeling. *Histochem. Cell Biol.* **106**, 41-58. doi:10.1007/BF02473201

Lloyd, T. E., Atkinson, R., Wu, M. N., Zhou, Y., Pennetta, G. and Bellen, H. J. (2002). Hrs regulates endosome membrane invagination and tyrosine kinase receptor signaling in *Drosophila*. *Cell* **108**, 261-269. doi:10.1016/S0092-8674(02)00611-6

Matsuda, S. and Affolter, M. (2017). Dpp from the anterior stripe of cells is crucial for the growth of the *Drosophila* wing disc. *eLife* **6**, e22319. doi:10.7554/eLife.22319

Mattila, P. E., Raghavan, V., Rbaibi, Y., Baty, C. J. and Weisz, O. A. (2014). Rab11a-positive compartments in proximal tubule cells sort fluid-phase and membrane cargo. *Am. J. Physiol. Cell Physiol.* **306**, C441-C449. doi:10.1152/ajpcell.00236.2013

Matusek, T., Wendler, F., Polès, S., Pizette, S., D'Angelo, G., Fürthauer, M. and Thérond, P. P. (2014). The ESCRT machinery regulates the secretion and long-range activity of Hedgehog. *Nature* **516**, 99-103. doi:10.1038/nature13847

Mc Dermott, R., Ziylan, U., Spehner, D., Bausinger, H., Lipsker, D., Mommaas, M., Cazenave, J.-P., Raposo, G., Goud, B., de la Salle, H. et al. (2002). Birbeck granules are subdomains of endosomal recycling compartment in human epidermal Langerhans cells, which form where Langerin accumulates. *Mol. Biol. Cell* **13**, 317-335. doi:10.1091/mbc.01-06-0300

Panáková, D., Sprong, H., Marois, E., Thiele, C. and Eaton, S. (2005). Lipoprotein particles are required for Hedgehog and Wingless signalling. *Nature* **435**, 58-65. doi:10.1038/nature03504

Pepinsky, R. B., Zeng, C., Wen, D., Rayhorn, P., Baker, D. P., Williams, K. P., Bixler, S. A., Ambrose, C. M., Garber, E. A., Miatkowski, K. et al. (1998). Identification of a palmitic acid-modified form of human Sonic Hedgehog. *J. Biol. Chem.* **273**, 14037-14045. doi:10.1074/jbc.273.22.14037

Petrov, K., Wierbowski, B. M., Liu, J. and Salic, A. (2020). Distinct cation gradients power cholesterol transport at different key points in the Hedgehog signaling pathway. *Dev. Cell* **55**, 314-327.e7. doi:10.1016/j.devcel.2020.08.002

Porter, J. A., von Kessler, D. P., Ekker, S. C., Young, K. E., Lee, J. J., Moses, K. and Beachy, P. A. (1995). The product of hedgehog autoproteolytic cleavage active in local and long-range signalling. *Nature* **374**, 363-366. doi:10.1038/374363a0

Rabouille, C., Kuntz, D. A., Lockyer, A., Watson, R., Signorelli, T., Rose, D. R., van den Heuvel, M. and Roberts, D. B. (1999). The *Drosophila* GMII gene encodes a Golgi alpha-mannosidase II. *J. Cell Sci.* **112**, 3319-3330.

Raftery, L. A., Sanicola, M., Blackman, R. K. and Gelbart, W. M. (1991). The relationship of decapentaplegic and engrailed expression in *Drosophila* imaginal disks: do these genes mark the anterior-posterior compartment boundary? *Development* **113**, 27-33. doi:10.1093/genetics/139.2.745

Ren, M., Xu, G., Zeng, J., De Lemos-Chiarandini, C., Adesnik, M. and Sabatini, D. D. (1998). Hydrolysis of GTP on rab11 is required for the direct delivery of transferrin from the pericentriolar recycling compartment to the cell surface but not from sorting endosomes. *Proc. Natl. Acad. Sci. USA* **95**, 6187-6192. doi:10.1073/pnas.95.11.6187

Sachse, M., Ramm, G., Strous, G. and Klumperman, J. (2002). Endosomes: multipurpose designs for integrating housekeeping and specialized tasks. *Histochem. Cell Biol.* **117**, 91-104. doi:10.1007/s00418-001-0348-0

Sanders, T. A., Llagostera, E. and Barna, M. (2013). Specialized filopodia direct long-range transport of SHH during vertebrate tissue patterning. *Nature* **497**, 628-632. doi:10.1038/nature12157

Sanicola, M., Sekelsky, J., Elson, S. and Gelbart, W. M. (1995). Drawing a stripe in *Drosophila* imaginal disks: negative regulation of decapentaplegic and patched expression by engrailed. *Genetics* **139**, 745-756. doi:10.1093/genetics/139.2.745

Slot, J. W. and Geuze, H. J. (2007). Cryosectioning and immunolabeling. *Nat. Protoc.* **2**, 2480-2491. doi:10.1038/nprot.2007.365

Sriram, V., Krishnan, K. S. and Mayor, S. (2003). deep-orange and carnation define distinct stages in late endosomal biogenesis in *Drosophila* melanogaster. *J. Cell Biol.* **161**, 593-607. doi:10.1083/jcb.200210166

Tanimoto, H., Itoh, S., ten Dijke, P. and Tabata, T. (2000). Hedgehog creates a gradient of DPP activity in *Drosophila* wing imaginal discs. *Mol. Cell* **5**, 59-71. doi:10.1016/S1097-2765(00)80403-7

Torroja, C., Gorfinkiel, N. and Guerrero, I. (2004). Patched controls the Hedgehog gradient by endocytosis in a dynamin-dependent manner, but this internalization does not play a major role in signal transduction. *Development* **131**, 2395-2408. doi:10.1242/dev.01102

Tukachinsky, H., Kuzmickas, R. P., Jao, C. Y., Liu, J. and Salic, A. (2012). Dispatched and scube mediate the efficient secretion of the cholesterol-modified hedgehog ligand. *Cell Rep.* **2**, 308-320. doi:10.1016/j.celrep.2012.07.010

Ullrich, O., Reinsch, S., Urbé, S., Zerial, M. and Parton, R. G. (1996). Rab11 regulates recycling through the pericentriolar recycling endosome. *J. Cell Biol.* **135**, 913-924. doi:10.1083/jcb.135.4.913

van der Beek, J., Jonker, C., van der Welle, R., Liv, N. and Klumperman, J. (2019). CORVET, CHEVI and HOPS - multisubunit tethers of the endo-lysosomal system in health and disease. *J. Cell Sci.* **132**, jcs189134. doi:10.1242/jcs.189134

Wang, X., Kumar, R., Navarre, J., Casanova, J. E. and Goldenring, J. R. (2000). Regulation of vesicle trafficking in madin-darby canine kidney cells by Rab11a and Rab25. *J. Biol. Chem.* **275**, 29138-29146. doi:10.1074/jbc.M004410200

Williams, M. A. and Fukuda, M. (1990). Accumulation of membrane glycoproteins in lysosomes requires a tyrosine residue at a particular position in the cytoplasmic tail. *J. Cell Biol.* **111**, 955-966. doi:10.1083/jcb.111.3.955

Suppl Figure 1: Pizette et al, 2021

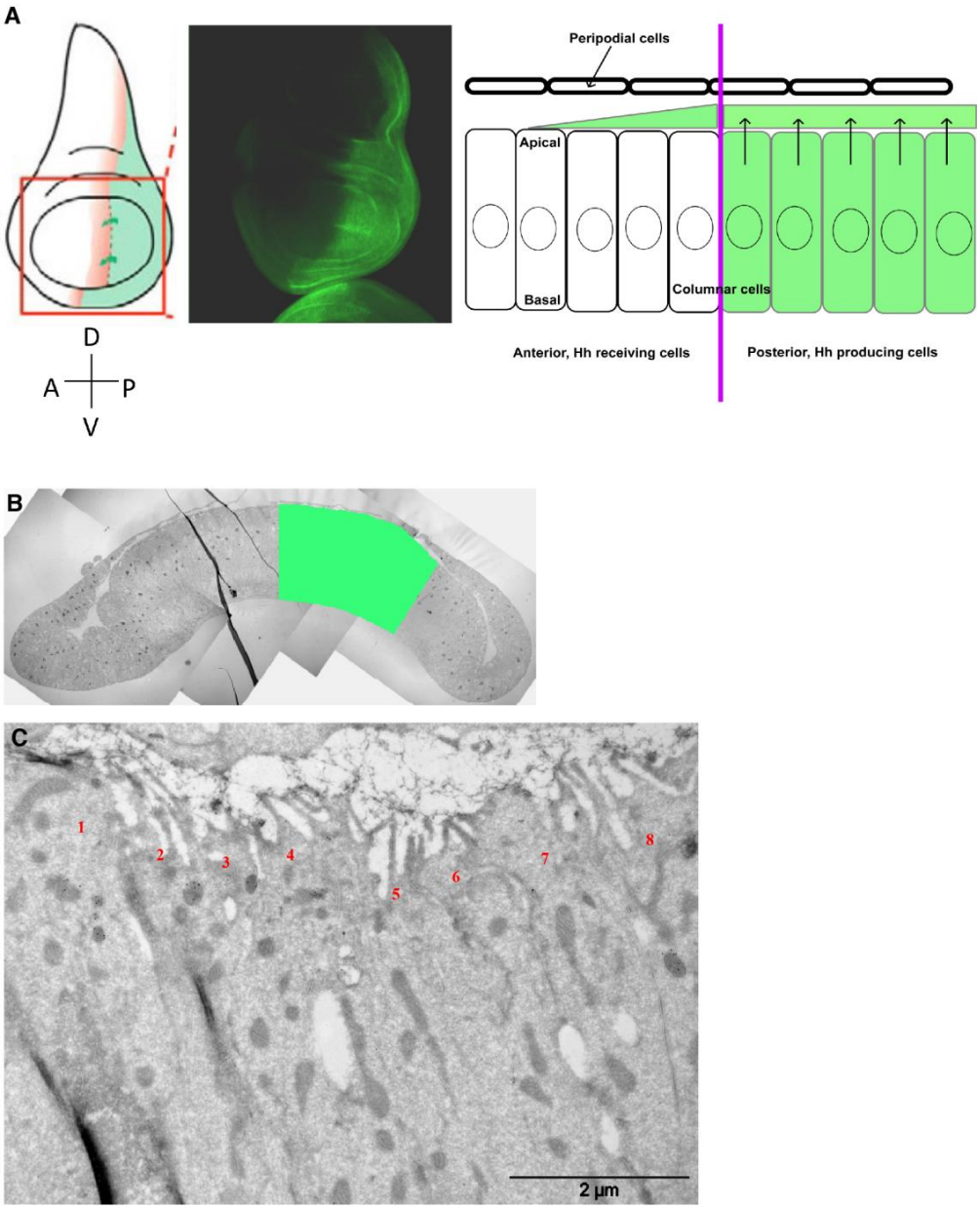

Figure S1: Hh production in the posterior compartment of Drosophila wing imaginal discs.

A: The left and middle panels present an overview of Hh production in the posterior compartment of the wing imaginal disc, in a schematic manner (left), and as an antibody staining by immunofluorescence (middle). The compass below the wing disc scheme displays the orientation of wing disc compartments. "A": Anterior; "P": Posterior; "D": Dorsal; "V": Ventral. Graded Hh target gene expression at the A/P compartment boundary is indicated in pink. The Hh producing cells are colored in green. The red square indicates the area of the wing disc pouch analysed at the ultrastructural level. The right panel depicts a schematic wing disc pouch sectioned along the Z plane. The posterior compartment as well as the Hh gradient is indicated in green. The A/P compartment boundary is marked with a purple line. Apical Hh secretion is indicated by black arrows.
B: Composite image of low magnification micrographs of an imaginal wing disc pouch frozen section along the Z plane. The posterior compartment is colored in green.
C: Zoomed micrograph of the posterior columnar epithelium on an disc ultrathin frozen section (as in B). Individual cells are marked by red numbers.

Suppl Figure 2: Pizette et al, 2021

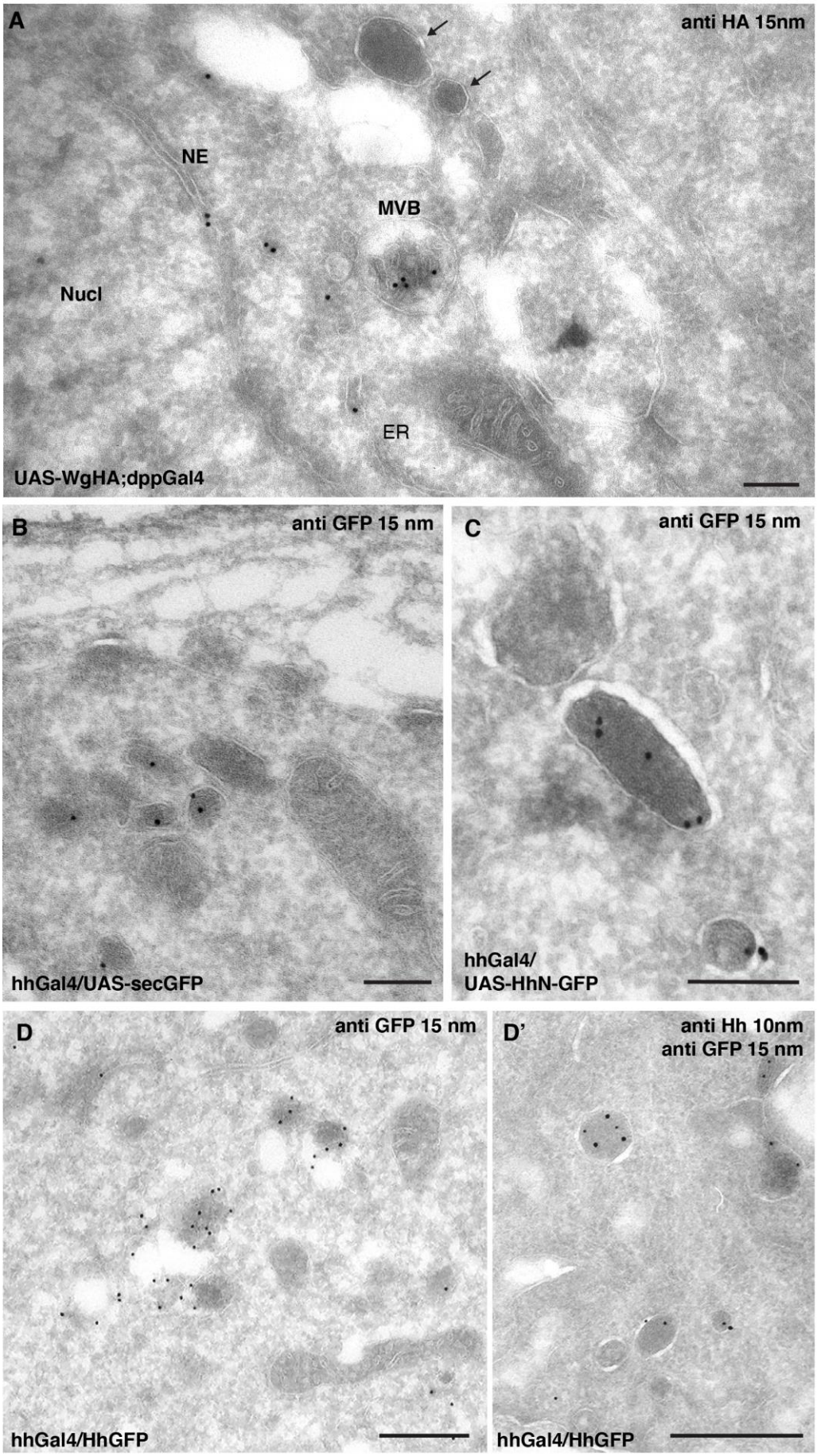

Figure S2: Hherisome formation is only driven by overexpression of untagged full length Hh.

A: Immunolocalisation of Wg-HA (anti HA, PAG 15 nm) expressed in the anterior cells of wing disc (dppGal4). Of note, WgHA was expressed using the dpp>gal4 driver, therefore leading to its expression within the Dpp expression domain that partly overlaps with part of the endogenous Wg domain. As we could not mark both domains simultaneously in this setting by IEM, we could not assess whether Wg reaches recycling endosomes within Wg producing cells or as a result of its internalization by Wg receiving cells. Note that Wg-HA is present in the endoplasmic reticulum (ER) and nuclear envelope (NE) as well as MVBs, but not in Hherisomes (arrows).

B, C, D: Immunolocalisation of posteriorly overexpressed secreted GFP (secGFP, B), of a truncated non-lipidated form of Hh, (HhN-GFP, C) and of a dually lipidated Hh tagged with GFP (HhGFP, D) with anti GFP followed by 15 nm PAG. Note that the density of these factors in Hherisomes remains low and that the number of Hherisomes does not appear boosted.

Nucl, Nucleus; PAG, protein A gold.

Scale bar: 200nm.

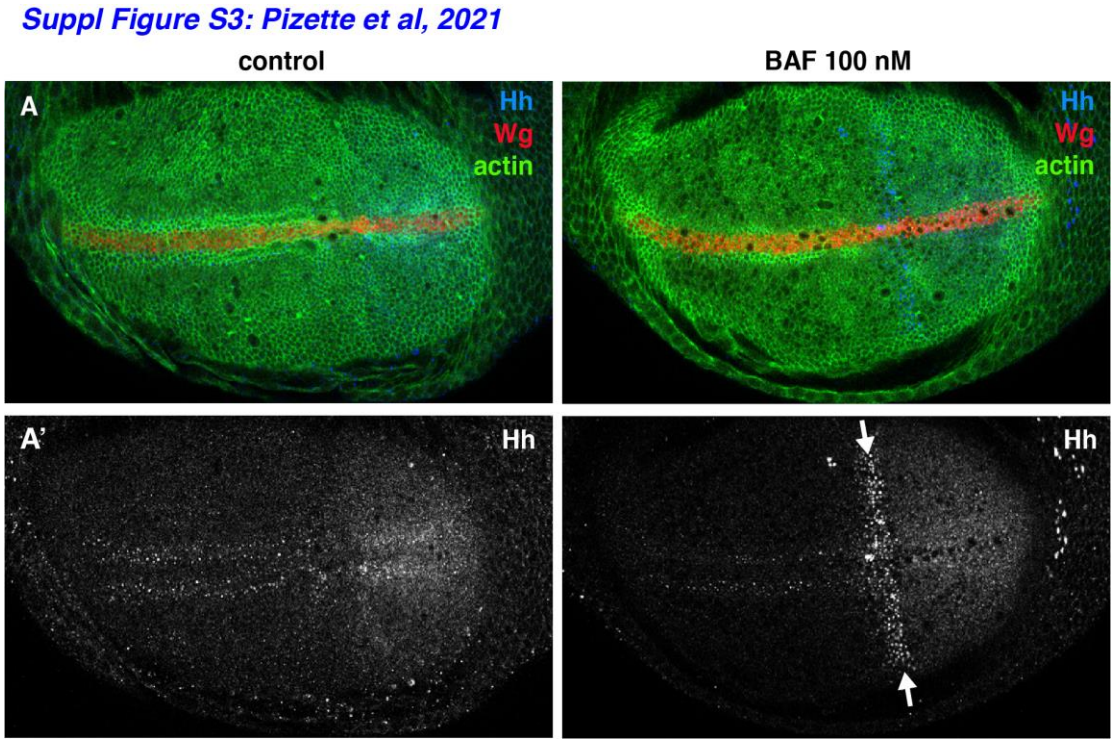

Figure S3: Endogenous Hh is not degraded in lysosomes.

A, A': Immunofluorescence staining of endogenous Hh (blue in A, white in A') in wing discs treated or not with 100nM Bafilomycin for 1h. Note that Hh intensity in the posterior compartment is not significantly changed between the two conditions, but strongly changed in the first proximal anterior cells. Arrows indicate the increase of Hh in A cells close to the A/P border. Actin, green; Wg, red.

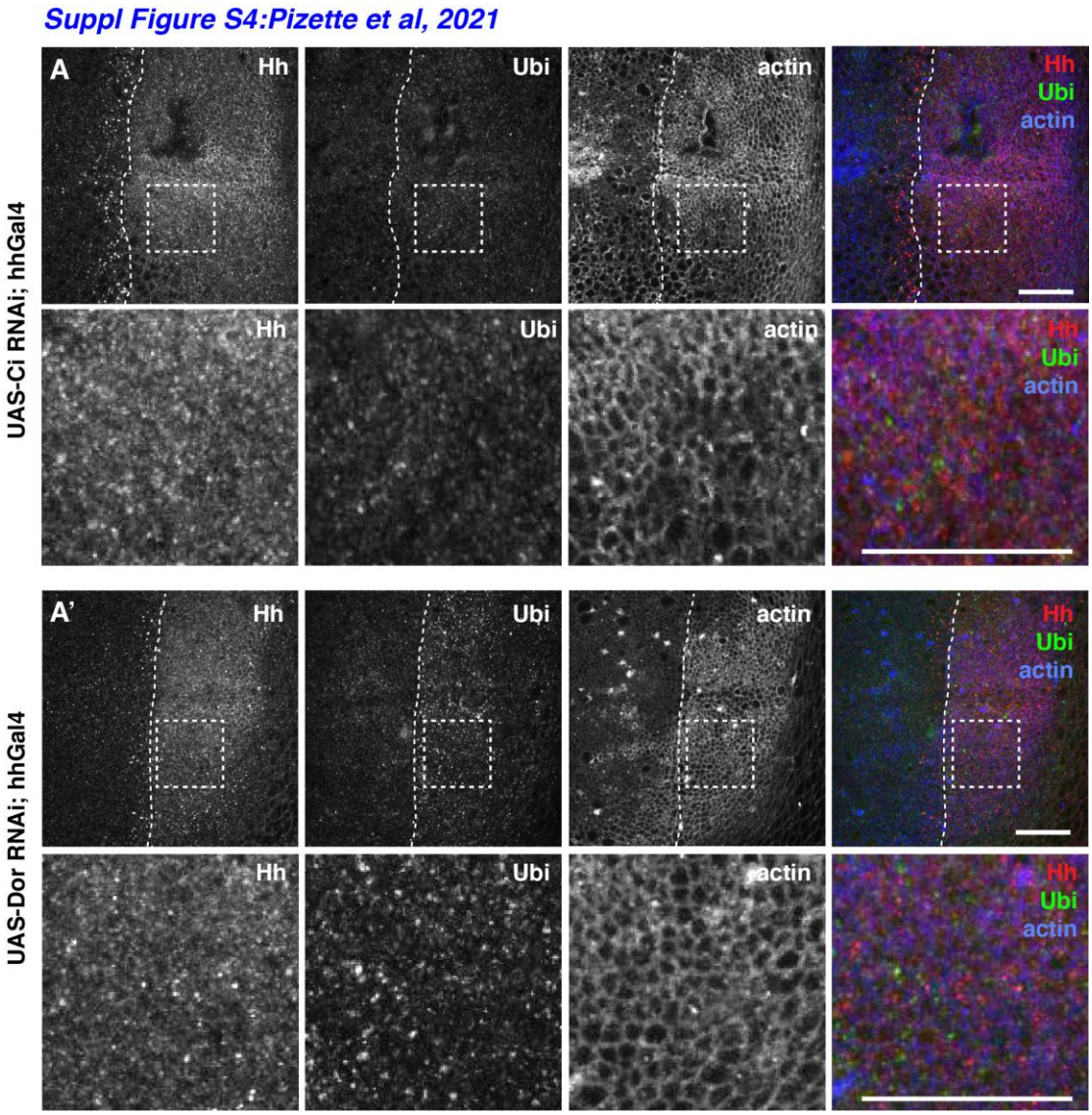

Figure S4: Endogenous Hh is not degraded in a Dor dependent manner.

A, A': Immunofluorescence staining of endogenous Hh (red), ubiquitinated proteins (green) and actin (blue) in wing imaginal discs where either Ci (UAS-Ci RNAi against Cubitus interruptus, A) or Dor (A') was depleted by RNAi in the posterior compartment. Note that Ci is not endogenously expressed in the posterior compartment. We did not observe any cell viability or growth defects using UAS-Ci RNAi therefore it serves as a neutral UAS control here and on *Suppl Figure S5*. Note, that while the Hh staining intensity is not significantly changed, the level of ubiquitinated proteins is elevated in the posterior compartment expressing Dor RNAi (A'). Posterior is right of the white dashed line that marks the A/P border (see *Suppl Figure S1*). Magnification of squared areas (dotted boxes in A and A') are presented below the panels.

Scale bar: 20µm.

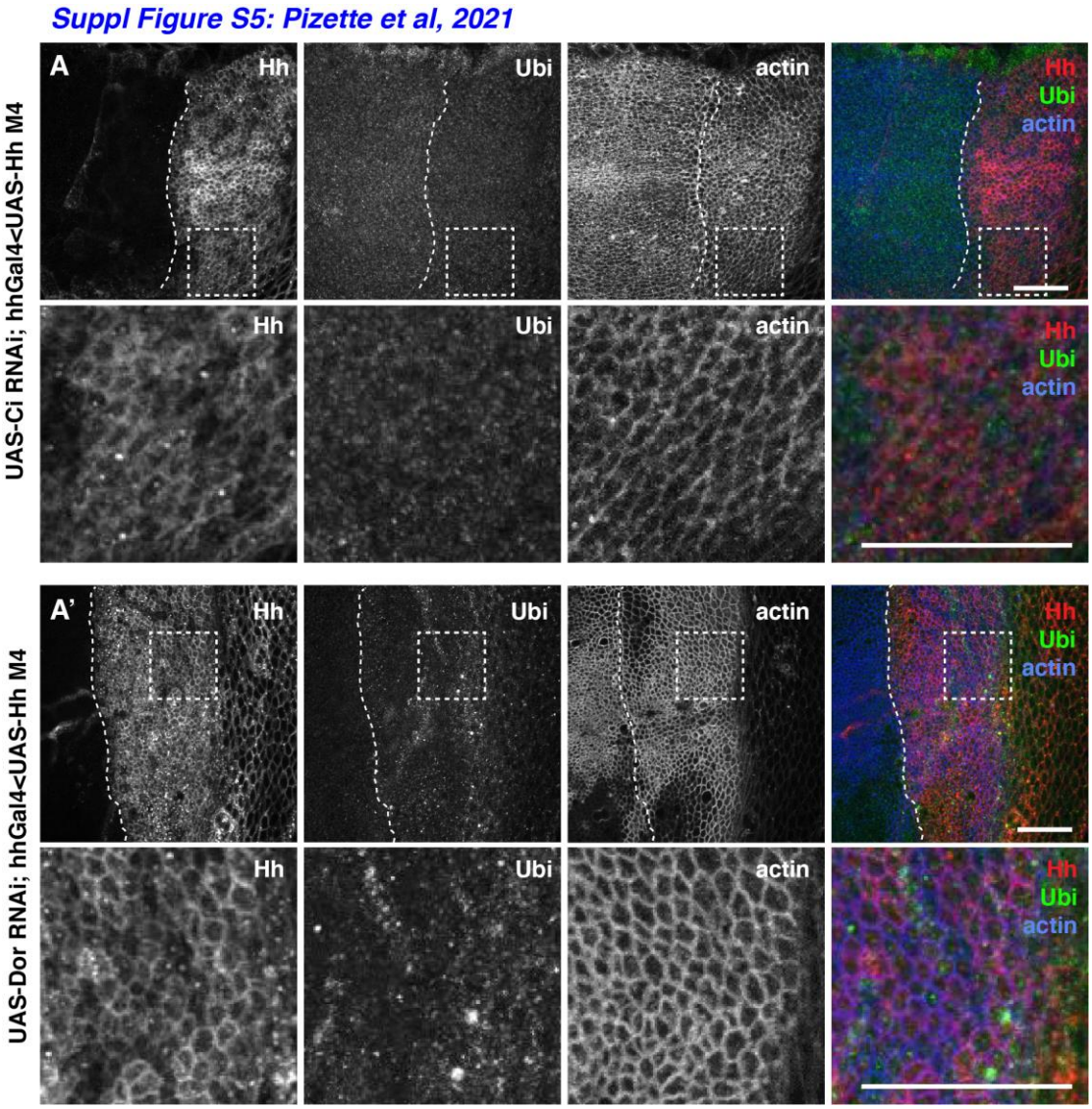

Figure S5: Overexpressed Hh is not degraded in a Dor dependent manner.

A, A': Immunofluorescence staining of overexpressed Hh (red), ubiquitinated proteins (green) and actin (blue) in wing imaginal discs where either Ci (UAS-Ci RNAi against Cubitus interruptus, A) or Dor (A') was depleted by RNAi in the posterior compartment. Note, that while the Hh staining intensity is not significantly changed, the level of ubiquitinated proteins is elevated in the posterior compartment expressing Dor RNAi (A'). Posterior is right of the white dashed line. Magnification of squared areas (dotted boxes in A and A') are presented below the panels.

Scale bar: 20µm.

Suppl Figure S6. Pizette et al, 2021

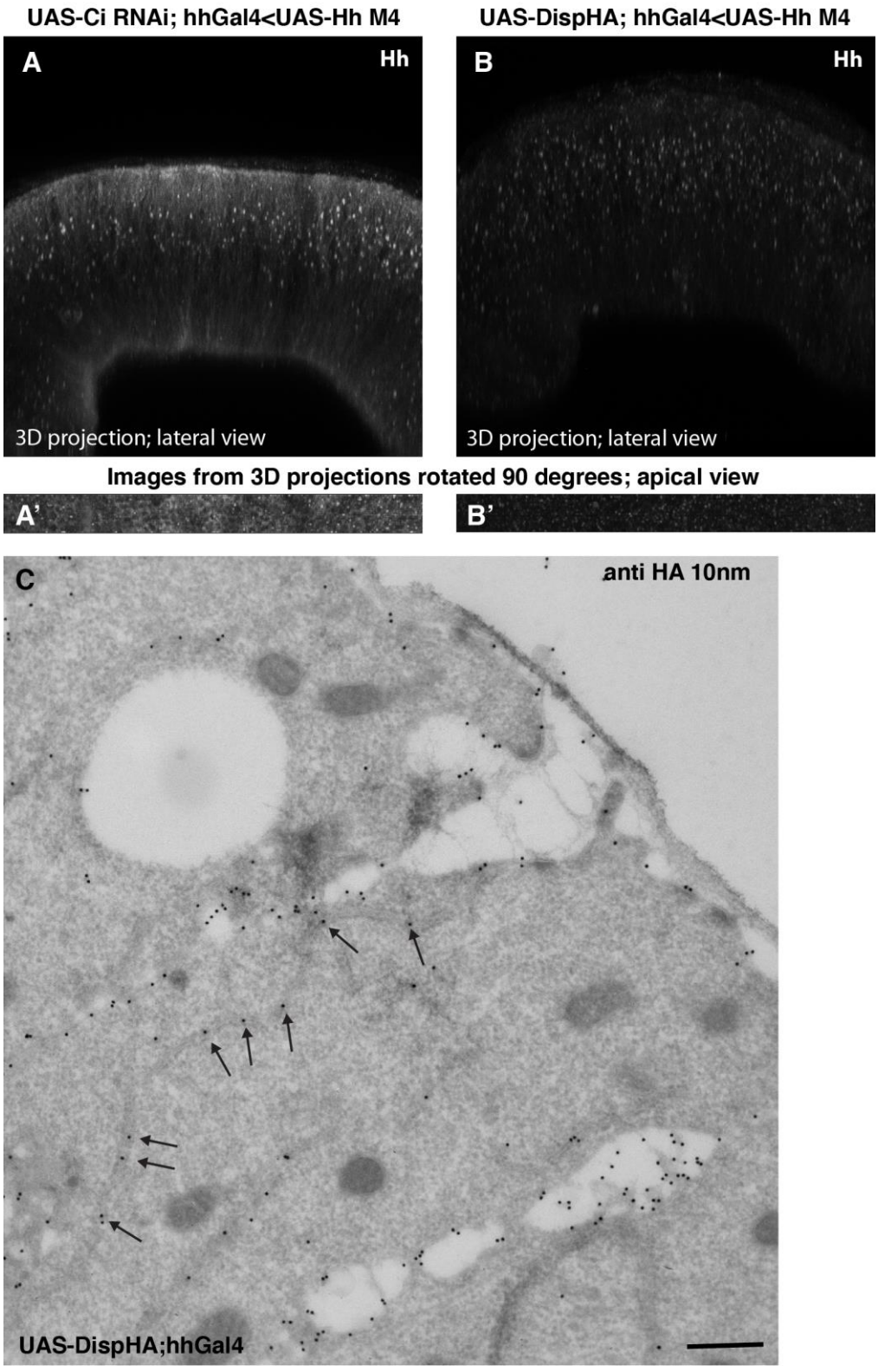

Figure S6: Disp is localized to the plasma membrane and its overexpression leads to less Hh at the plasma membrane.

A-B': 3D reconstructions generated from posterior optical sections from a 10µm wide Z volume. Images were taken at the same time using the same acquisition settings.

A and B are lateral views of control (A) and DispHA (B) overexpressing discs (in the posterior compartment), while their corresponding apical view is shown on A' and B'. Note that Hh is less present at the plasma membrane in DispHA and Hh co-overexpressing discs when compared to UAS-Ci RNAi that was used as a neutral tool for UAS dosage control. **C**: Immunolocalisation of DispHA (HA, 10 nm PAG) on the posterior disc cells where it is specifically overexpressed. Examples of labelling at the basolateral plasma membrane is marked with black arrows. As control for the labeling specificity, we analyzed the anterior cells and did not observe any HA staining (data not shown).

Scale bar: 200nm.

Suppl Figure S7: Pizette et al, 2021

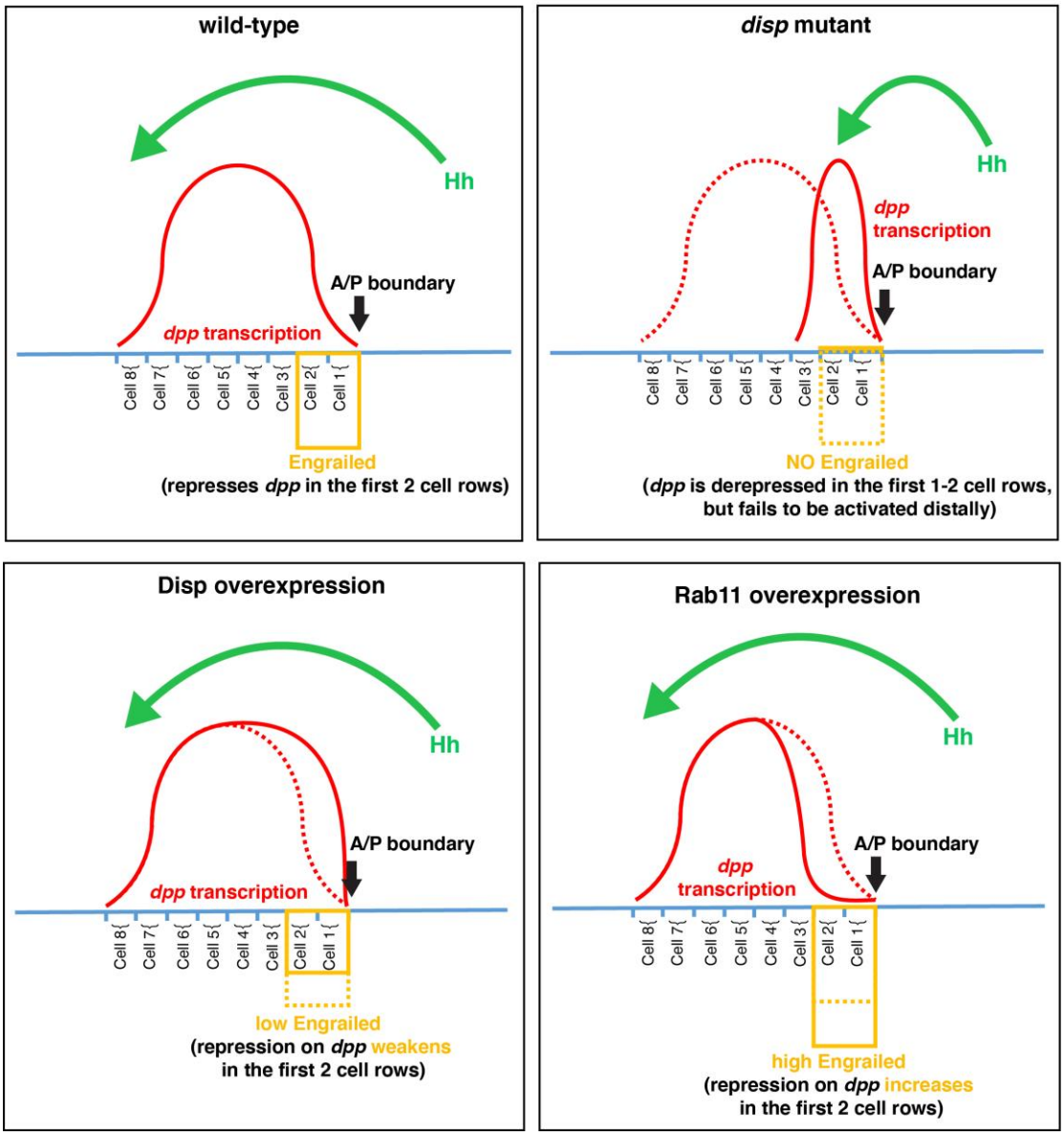

Figure S7: Schematic representation of dpp expression pattern and En expression levels in different backgrounds.

The blue line represents the columnar epithelium of wing imaginal disc pouch, where posterior is to the right. Green arrows represent the spread of the Hh gradient. *dpp* transcription is shown with the solid red line in all backgrounds. The wild type *dpp* transcriptional pattern is marked with a dotted red line in the mutant contexts for comparison. The anterior Engrailed (En) expression level is indicated with a yellow rectangle at the anterior side of the A/P margin (black arrows) in all backgrounds. The wild type En is marked in dashed yellow squares in the mutant backgrounds for comparison. Note that the height of the yellow squares indicate the difference in En expression level in Disp and Rab11 overexpression compared to *wild type*, and that anterior En expression is absent in *disp* mutant.

Suppl Figure S8: Pizette et al, 2021

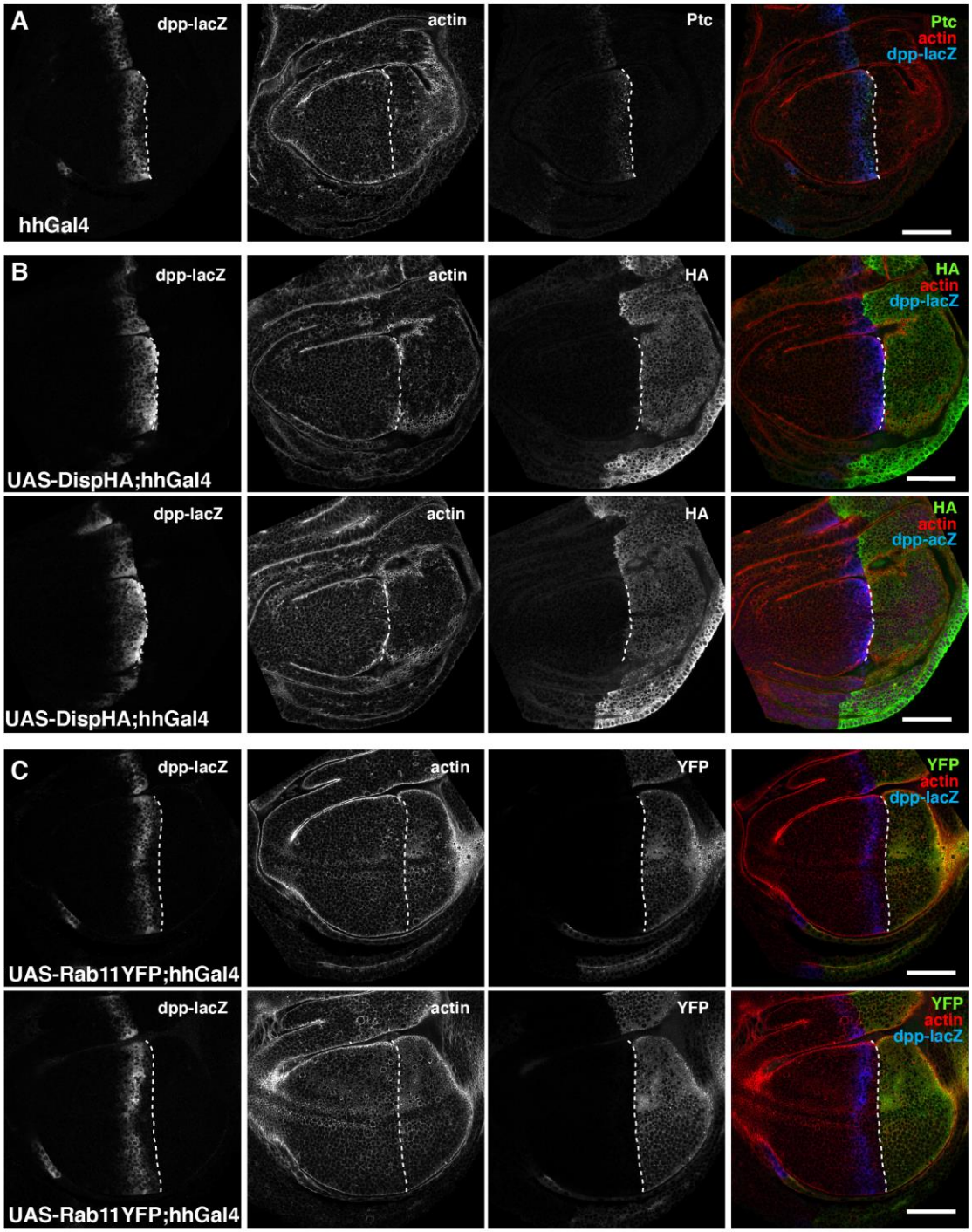

Figure S8: Additional examples of differential modification of Hh target gene expression patterns in Disp and Rab11 overexpressors.

A-C: Expression patterns of *dpp-lacZ* in *wild type* (A), Disp overexpressing discs (B) and Rab11 overexpressing (C) wing discs. The demarcation of the A/P boundary (white dashed lines) is achieved with Ptc immunostaining in the control, and with YFP (for Rab11) or HA (Disp) immunolabeling (green channels in the rightmost column).

Scale bar: 50µm.

Table S1: Number of Hherisomes and Hh labeling density in wild type discs and upon Hh and Hh-GFP overexpression in the posterior disc compartment

Genotype	Numbers of Hherisomes profiles/disc cell	Hh Labeling density in Hherisomes/µm^2 (as in Table 1)	Size (nm)
OreR	1	73.5±50	125±78
hhGal4/UAS-Hh **M4**	4.2	520±30	205±130
Fold increase	4.2	7	2
hhGal4/UAS-Hh**GFP**	1.25	94±10 (anti-GFP) ***105*** (anti-Hh) in double labeling	ND
Fold increase	1.25	1.16-1.28	

Table S2: Accessibility of Hherisomes to endocytosed BSA-gold

		% (basal*) Hherisomes positive for BSA-gold	% (basal*) endosomes positive for BSA-gold
1h uptake	posterior	14.7%	100%
1h uptake + 2h chase	posterior	14.6%	100%
1h uptake + 4h chase	posterior	18.7%	100%

* : Due to the presence of the squamous layer of cells (peripodial) covering the apical side of the epithelial disc cells, the uptake of BSA-gold is delayed when compared to the basal side. Consequently, only the basal side of the disc cells was assessed.

Table S3: Number of Hherisomes and Hh labeling density in Hherisomes upon Rab11 and Disp overexpression

Genotype	Number of Hherisome profiles/ per 10µm^2 (of positive fields)	Hh Labeling density in Hherisomes/µm^2 (as in Table 1)
UAS Hh**M1;** hhGal4	Post: 2.75 Ant: 1.25	328±25 159±40
UAS-**Hh M1**;hhGal4/ UAS-Rab11YFP	Post: 2.35 Ant: 2.6	721±90 362±100
UAS-DispHA;hhGal4/ UAS-**Hh M4**	Post: 0.15 Ant: nd	ND 142.5±40

Table S4: Crosses set up for Hh signaling and growth experiments and IEM studies

Final genotype	Paternal genotype	Maternal genotype	Figure/Table
OreR	*OreR*/Y	*OreR*	*1,3, S1, Table 1, Table S1*
w^{1118}	w^{1118}/Y	w^{1118}	*S3, 7*
w^{1118};*dpp-LacZ/+;UAS-Hh(M4)/hhGal4*	w^{1118}/Y;*UAS-Hh(M4)*	w^{1118};*dpp-lacZ;hhGal4/TM6b*	*1, 3, 4, TableS1, Table S2*
w^{1118};*UAS-*Wg^{HA}*/+;dppGal4/+*	w^{1118}/Y;*UAS-*Wg^{HA}*/CyO*	w^{1118};*dppGal4/TM6b*	*S2*
w^{1118};*apGal4/+;UAS-cytoGFP<UAS-Hh(M4)/+*	w^{1118}/Y;*UAS-cytoGFP<UAS-Hh(M4)*	w^{1118};*apGal4/BcG*	*2*
w^{1118};*UAS-*Ptc^{1130X}*/dpp-lacZ;UAS-Hh(M4)/ hhGal4*	w^{1118}/Y;*UAS-*Ptc^{1130X}*;UAS-Hh(M4)*	w^{1118};*dpp-lacZ;hhGal4/TM6b*	*Table1*
w^{1118};*UAS-Hh(M1)/dpp-LacZ;UAS-HRP-hLamp1/hhGal4*	w^{1118}/Y;*UAS-Hh (M1);UAS-HRP-hLamp1b*		*3, Table1, Table S3*
w^{1118};*dpp-lacZ/+;UAS-HhN-GFP/hhGal4*	w^{1118}/Y;*UAS-HhN-GFP*		*S2*
w^{1118};*dpp-lacZ/+;UAS-secGFP/hhGal4*	w^{1118}/Y;*UAS-secGFP/TM3,Sb*		*S2*
w^{1118};*dpp-lacZ/+;UAS-cytoGFP<UAS-Hh(M4)/hhGal4*	w^{1118}/Y;*UAS-cytoGFP<UAS-Hh(M4)*		*2, Table1*
w^{1118};*UAS-Hh(M1)/dpp-lacZ;UAS-Rab11-YFP/hhGal4*	w^{1118}/Y;*UAS-Hh(M1);UAS-Rab11-YFP/SM6-TM6b*		*4, Table1*
w^{1118};*UAS-*$Disp^{HA}$*/dpp-lacZ;hhGal4/+*	w^{1118}/Y;*UAS-*$Disp^{HA}$*/ CyO,KrGal4,UAS-GFP*		*S6*
w^{1118};*UAS-*$Disp^{HA}$*/dpp-lacZ;UAS-Hh(M4)/ hhGal4*	w^{1118}/Y; *UAS-*$Disp^{HA}$*;UAS-Hh(M4)/ SM6-TM6b*		*5, Table1, Table S3*
w^{1118}*; UAS-Hh-GFP/dpp-lacZ;hhGal4/+*	*y,*w^{1118}/Y;*UAS-Hh-GFP*		*S2, TableS1*
w^{1118};*dpp-lacZ;FRT82disp*^{SO37707}	w^{1118}/Y;*dpp-lacZ; FRT82disp*^{SO37707}*/TM6b*	w^{1118};*dpp-lacZ; FRT82,disp*^{SO37707}*/TM6b*	*5*
w^{1118};*UAS-cytoGFP<UAS-Hh(M1)/dpp-lacZ;FRT82,disp*^{SO37707}*/hhGal4<FRT82,disp*^{SO37707}	w^{1118}/Y;*UAS-cytoGFP<UAS-Hh(M1)/CyO;FRT82,disp*^{SO37707}*/TM6b*	w^{1118};*dpp-lacZ; hhGal4<FRT82,disp*^{SO37707}*/TM6b*	*5, Table1*
w^{1118}*; UAS-Ci* RNAi */tubGal80*^{ts}*; hhGal4<UAS-Hh(M4)/+*	*y,*w^{1118}/Y;*UAS-Ci* RNAi	w^{1118};*tubGal80*^{ts}*;hhGal4<UAS-Hh (M4)/TM6b,Tb*	*S5, S6*
w^{1118}*; UAS-dor* RNAi/ *tubGal80*^{ts}*; hhGal4<UAS-Hh(M4)/+*	*y,*w^{1118}/Y;*UAS-dor* RNAi		*S5*
w^{1118}*; UAS-Disp*^{HA}*/ tubGal80*^{ts}*; hhGal4<UAS-Hh(M4)/+*	w^{1118}/Y;*UAS-Disp*^{HA}*/CyO*		*S6*
w^{1118}*; UAS-Ci* RNAi */ tubGal80*^{ts}*<dpp-lacZ; hhGal4/+*	*y,*w^{1118}/Y;*UAS-Ci* RNAi	w^{1118};*tubGal80*^{ts}*<dpp-lacZ; hhGal4/ TM6b,Tb*	*S4*
w^{1118}*; UAS-dor* RNAi/ *tubGal80*^{ts}*<dpp-lacZ; hhGal4/+*	*y,*w^{1118}/Y;*UAS-dor* RNAi		*S4*
w^{1118};*UAS-Disp*^{HA}*/ tubGal80*^{ts}*<dpp-lacZ; hhGal4/+*	w^{1118}/Y;*UAS-Disp*^{HA}*/CyO*		*6, S8, 7*
w^{1118}*; UAS-Rab11-YFP/ tubGal80*^{ts}*<dpp-lacZ; hhGal4/+*	w^{1118}/Y;*UAS-Rab11-YFP/CyO*		*6, S8, 7*
w^{1118}*; tubGal80*^{ts}*<dpp-lacZ/+;hhGal4/+*	w^{1118}/Y		*6, S8, 7*
w^{1118}*; UAS-Disp*^{HA} */enGal4< tubGal80*^{ts}*; hh*^{ts2}*/ hh*^{ts2}	w^{1118}/Y;*UAS-Disp*^{HA}*;hh*^{ts2}*/SM6-TM6b*	w^{1118}*; enGal4<tubGal80*^{ts}*; hh*^{ts2}*/ SM6-TM6b*	*7*
w^{1118}*; UAS-Rab11-YFP /enGal4< tubGal80*^{ts}*; hh*^{ts2}*/ hh*^{ts2}	w^{1118}/Y; *UAS-Rab11-YFP; hh*^{ts2}*/SM6-TM6b*		*7*
w^{1118}*; enGal4< tubGal80*^{ts}*/+; hh*^{ts2}*/ hh*^{ts2}	w^{1118}/Y;*hh*^{ts2}*/TM6b,Tb*		*7*
w^{1118}*; UAS-Rab11-YFP/ tubGal80*^{ts}*<dpp-lacZ; disp*^{SO37707}*/ hhGal4<disp*^{SO37707}	w^{1118}/Y; *UAS-Rab11-YFP; disp*^{SO37707}*/SM6-TM6b*	w^{1118}*; tubGal80*^{ts}*<dpp-lacZ; hhGal4<disp*^{SO37707}*/TM6b,Tb*	*7*
w^{1118}*; dpp-lacZ / tubGal80*^{ts}*; disp*^{SO37707}*/ hhGal4<disp*^{SO37707}	w^{1118}/Y; *dpp-lacZ; disp*^{SO37707}*/TM6b,Tb*	w^{1118}*; tubGal80*^{ts}*; hhGal4<disp*^{SO37707}*/TM6b,Tb*	*7*